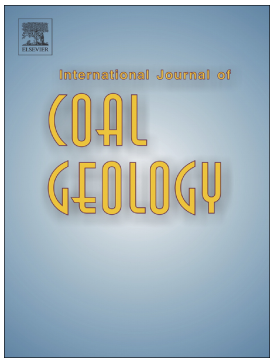

Organic matter provenance and depositional environment of marine-to-continental mudstones and coals in eastern Ordos Basin, China—Evidence from molecular geochemistry and petrology

Yu Qi, Yiwen Ju, Jingqiang Tan, Leon Bowen, Chunfang Cai, Kun Yu, Hongjian Zhu, Cheng Huang, Weilai Zhang

PII: S0166-5162(19)30377-5

DOI: https://doi.org/10.1016/j.coal.2019.103345

Reference: COGEL 103345

To appear in: *International Journal of Coal Geology*

Received date: 4 April 2019

Revised date: 26 August 2019

Accepted date: 12 November 2019

Please cite this article as: Y. Qi, Y. Ju, J. Tan, et al., Organic matter provenance and depositional environment of marine-to-continental mudstones and coals in eastern Ordos Basin, China—Evidence from molecular geochemistry and petrology, *International Journal of Coal Geology*(2018), https://doi.org/10.1016/j.coal.2019.103345

Organic matter provenance and depositional environment of marine-to-continental mudstones and coals in eastern Ordos Basin, China—evidence from molecular geochemistry and petrology

Yu Qi[1,2], Yiwen Ju[1,*] juyw03@163.com, Jingqiang Tan[3], Leon Bowen[4], Chunfang Cai[5], Kun Yu[1], Hongjian Zhu[1], Cheng Huang[1], Weilai Zhang[6]

[1]Key Laboratory of Computational Geodynamics, College of Earth and Planetary Sciences, University of Chinese Academy of Sciences, Beijing 100049, China

[2]Department of Earth Sciences, Durham University, Durham DH1 3LE, UK

[3]School of Geosciences and Info-physics, Central South University, Changsha 410012, China

[4]Department of Physics, Durham University, South Road, Durham DH1 3LE, UK

[5]Key Laboratory of Petroleum Resources Research, Institute of Geology and Geophysics, Chinese Academy of Sciences, Beijing 100029, China

[6]State Key Laboratory of Heavy Oil Processing, China University of Petroleum, Beijing 102249, China

[*]Corresponding author.

Abstract

Cyclothems, composed of interbedded mudstone, coal and sandstone layers, make up the Taiyuan and Shanxi Formations in the Late Carboniferous to Early Permian in North China under a marine-to-continental depositional environment. The cyclothems act as important fossil energy hosts, such as coalbeds, hydrocarbon source rocks and unconventional natural gas reservoirs. Organic geochemistry and petrology of mudstones and coals in the Taiyuan and Shanxi Formations in the eastern Ordos Basin were studied to reveal the organic matter sources and paleoenvironments. Total organic carbon (TOC) contents vary from 1.1 wt.% (mudstone) to 72.6 wt.% (coal). The samples are mainly within the oil window, with the T_{max} values ranging from 433 to 469°C. Organic petrology and source biomarkers indicate that the mudstones were sourced from a mixed organic matter input, and terrigenous organic matter predominates over aquatic organic matter. The coals are mostly sourced by terrigenous organic matter inputs. High concentrations of hopanes argue for a strong bacterial input. Some m/z 217 mass chromatograms have peaks at the hopanes' retention times as a result of high hopane to sterane ratios. These hopane-derived peaks do not interfere the identification of the steranes because the hopanes and the steranes have different retention times. Maturity-dependent biomarkers demonstrate that the samples have been thermally mature, which agree with the T_{max} values. Anomalously low C_{29} 20S/(20S+20R) and C_{29} ββ/(ββ+αα) sterane ratios are

present in all the samples, and are interpreted as due to the terrigenous organic matter input or the coal-related depositional environment. In addition, biomarkers and iron sulfide morphology indicate that the organic matter of the mudstones deposited in a proximal setting with shallow, brackish/fresh water bodies. With consideration of preservation of organic matter, the redox conditions are dysoxic. Redox oscillations resulted in the records of oxic conditions in some samples. Finally, the coals and the mudstones mainly generate gas and have poor oil generative potential.

Keywords: Organic geochemistry, Organic petrology, Pyrite, Organic matter provenance, Mudstone, Coal, Ordos Basin

1 Introduction

Taiyuan and Shanxi Formations in Late Carboniferous to Early Permian in the eastern Ordos Basin are coal measures and act as important fossil energy hosts, such as coalbeds, hydrocarbon source rocks and unconventional natural gas reservoirs (Xiao et al., 2005). Tight gas and coalbed methane in the formations in Linxing, eastern Ordos Basin have been commercially developed (Meng et al., 2018; Qi et al., 2019b). Joint developments of tight gas, coalbed methane and shale gas have been proposed and tested to increase the efficiency of gas recovery (Ju et al., 2014; Li et al., 2016; Ju et al., 2018; Li et al., 2019). In addition, the coals and shales in the formations have been found to be the dominant source rocks for the tight gas pools in almost all huge gas fields in the Ordos Basin, such as Sulige, Daniudi and Wushenqi gas fields. However, the organic matter provenance and depositional environment of the source rocks (including organic-rich mudstones and coals) remain unclear, which will result in inaccurate estimations of hydrocarbon potential (Hu et al., 2018).

Organic petrology and organic geochemistry play important roles in determining organic matter provenance, thermal maturities and paleo-depositional environments (Jiamo et al., 1990; Hasiah and Abolins, 1998; Holba et al., 2003; Böcker et al., 2013; French et al., 2014; Hackley et al., 2016; Hakimi and Ahmed, 2016; Adebayo et al., 2018; Ghassal et al., 2018; Zieger and Littke, 2019). A lot of organic geochemical studies on marine shales have been done, but transitional source rocks are inadequately studied. Many marine shales, especially shallow marine shales, have been found to contain humic organic matter, generally with a lower concentration than the aquatic organic matter (Milliken et al., 2013; Mathia et al., 2016; Adegoke et al., 2017; Petersen et al., 2017; Borrego et al., 2018). The organic matter input of transitional source rocks is more complex. Previous studies have shown that mudstones and interbedded coals may exhibit considerable variations in kerogen types (e.g. algal organic matter vs

land plant) and depositional environments, especially marine-affected coal measures (Sun et al., 2000; Rangel et al., 2002). Various kerogen types also lead to a wide range of HI values of coal measures (see also Wu et al., 2018). Carbon isotope compositions and biomarkers, such as Pr/Ph and gammacerane indices, can differentiate the mudstones and the interbedded coals (Hasiah and Abolins, 1998; Kotarba and Clayton, 2003; Zhu et al., 2012; Adegoke et al., 2015). The mudstones are commonly found to deposit in more reducing conditions than the coals. In addition, iron sulfides are also key indicators of contemporary environmental conditions (Rickard and Luther, 2007). Iron sulfides occur in sediments from deep sea to non-marine, and the principal iron sulfide in rock records is pyrite (Schieber, 2011a). Pyrite morphology reveals whether it is formed during deposition period, early diagenesis or late diagenesis (Kortenski and Kostova, 1996; Wilkin et al., 1996, Wilkin et al., 1997). Diameters of framboids were found to decrease with increasing reducing conditions (Wilkin et al., 1996).

This study is to understand the provenance and depositional environments of the organic matter in the Late Carboniferous to Early Permian in the Linxing Area of the eastern Ordos Basin. Detailed molecular geochemistry of mudstones and coals is studied for the first time in the Taiyuan and Shanxi Formations in Eastern Ordos Basin. Organic geochemistry is also integrated with organic petrology and SEM observation. This study is of significance to estimating the hydrocarbon potential of the source rocks in the Linxing Area, and also helps understand the accumulation and preservation of organic matter in the cyclothems in the eastern Ordos Basin.

2 Geologic setting and sampling

The Ordos Basin is located in the western part of the North China Block, bordered by the Yin Mountain, Lvliang Mountain, Qinling Mountain, and Liupan and Helan Mountains (Figure 1a). It was formed on Archean granulites and lower Proterozoic greenschists of the North China Block (Zhang, 1989), and has experienced four evolutionary stages: The Early Palaeozoic shallow marine platform, the Late Palaeozoic offshore plain, the Mesozoic intracontinental basin and the Cenozoic faulting and subsidence (Yang et al., 2005). The eastern Ordos Basin entered into a marine-to-continental depositional environment in the Late Carboniferous and Early Permian. Alternating regression and transgression occurred during the transitional period. Typical cyclothems deposited as the Taiyuan and Shanxi Formations, including several coal seams and thick organic-rich mudstone layers (Figure 2).

The sampling area is the Linxing Area in the eastern Ordos Basin (Figure 1a). The Linxing Area is situated at 38° northern latitude, which is the “fulcrum” of the north-south “seesaw” of the Ordos Basin (Li et al., 2012). The

"fulcrum" acts as a transitional zone between marine and continental depositional environments, with paleo-water depths increasing from north to south (Li et al., 2012). Organic matter of the mudstones in the Linxing Area includes both type II_2 and III kerogen (Li et al., 2016). No.8 (+9+10) and No. 5 (+3+4) coalbeds are regionally (or locally) workable coalbeds (Li et al., 2016). Thirteen mudstones, including five coal-lamina-bearing mudstones (coaly mudstones), and six coals were collected from different fresh coalfaces and drilling faces of six underground coal mines with depths between 153-390 m to escape from weathering. Table 1 shows the formations that the samples belongs to. The locations of the coal mines are shown in Figure 1b.

3 Methods

Total organic carbon (TOC) analysis and Rock-Eval pyrolysis were performed on all the samples. TOC was measured with a LECO CS230 Carbon/Sulfur analyzer after removing carbonate in the samples with hydrochloric acid (HCl). Pyrolysis was performed using Rock-Eval 6 equipment. Pyrolysis parameters, like free hydrocarbons (S_1, mg HC/g rock), hydrocarbon generation potential (S_2, mg HC/g rock), temperature of maximum pyrolysis yield (T_{max}, °C) and hydrogen index (HI, mg HC/g TOC), were recorded or calculated.

Macerals of the coals and the mudstones were investigated under plane polarized reflected light with a fluorescence illuminator. All images were taken under a Leica Plan 50×/0.85 oil immersion objective to acquire 500× magnification. Maceral compositions were determined under both incident white light and UV light. Vitrinite reflectance (R_o) of the coals was measured on the coal samples prepared following ASTM standard D2797. R_o was examined in incident white light at magnification of 500× oil immersion.

Mechanically polished thin sections were also prepared for the mudstone samples. A Hitachi SU-70 High Resolution Analytical Scanning Electron Microscope (SEM) equipped with an Oxford Instrument Energy Dispersive Spectrometer (EDS) was used to observe the thin sections after applying a sputter coating of ~20 nm thickness of carbon. Secondary imagery was taken under 15kV and a working distance of ~15mm. Mineral components were confirmed by X-ray energy dispersive spectrums.

Molecular geochemistry was studied by gas chromatography (GC) and gas chromatography mass spectrometry (GC-MS) in the State Key Laboratory for Heavy Oil Processing, China. Coaly mudstones were excluded to avoid the influence of intercalated coal laminae. The mudstones and the coals were solvent-extracted by a Soxhlet extractor with a solvent mixture of dichloromethane and methanol (volume ratio 9:1). The samples were refluxed for more than 96 hours until the effluent distilled solvent was colourless and transparent. Group

components were separated from the extracts by liquid column chromatography. A chromatographic column (20× 0.80 cm) was packed 3 g of silica gel which has been activated at 200 ℃ for 4h and 2 g of alumina which has been activated at 400-450 ℃ for 4h. Both the silica gel and alumina are of 100-200 mesh. Normal hexane was used to elute saturated fractions. The coaly mudstones, namely the coal-laminae bearing mudstones, were excluded for GC and GC-MS analysis, because bulk biomarker analysis will mix the information of both the interbedded coal laminae and the mudstone matrix.

GC analysis of the saturated fractions was performed by a Gas Chromatography Flame Ionization Detector equipped with a HP-5 silica capillary column (30m×0.25mm×0.25μm). Oven temperature was initially set as 100 ℃ for 1 minute and was then increased to 300 ℃ with a step of 4 ℃/ min, followed by an isothermal period of 10 minutes. Gaseous saturated hydrocarbons were carried by 99.999 % Helium at a linear velocity of 1 mL/min.

GC-MS analysis of the saturated fractions was conducted by an Agilent 7890-5975c instrument also equipped with a HP-5 silica capillary column (30m×0.25mm×0.25μm). Oven temperature was initially set as 50 ℃ for 1 minute, and was increased to 120 ℃ with a step of 20 ℃/ min, then to 250 ℃ with a step of 4 ℃/min, and finally to 310 ℃ with a step of 3 ℃/min; the period at 310 ℃ was 30 min. Helium (99.999 %) was used as a carrier gas at a speed of 1 mL/min. The mass spectrometer was operated in electron ionization mode (EI) at 70 eV. The voltage of multiplier was 1200 V. All biomarkers ratios, except for C_{29} sterane maturity ratios, were calculated on the base of peak area integration above baseline of specific ion chromatograms. The C_{29} sterane maturity ratios was calculated from peak height to reduce the effects of co-elution.

4 Results

4.1 Bulk geochemical parameters

Results of bulk geochemical analysis are listed in Table 1. The TOC contents of the mudstones, the coaly mudstones and the coals are in the range of 1.1-8.4 wt.%, 15.6-22.2 wt.% and 55.8-72.6 wt.%, respectively. The samples are mainly within the oil window, with T_{max} values varying from 433 to 469 ℃. The R_o of the coals ranges from 0.78 % to 1.15 % and has a linear correlation with their T_{max} values (the R^2 of the linear fitting is 0.95). Thermal maturity of the samples generally increases from north to south. The HI values of the mudstones, the coaly mudstones and the coals are in the range of 17-111 mg HC/g TOC, 76-249 mg/g TOC and 129-269 mg/g TOC, respectively.

4.2 Organic petrology

According to organic petrological images, vitrinite and inertinite are dominant macerals, especially for the coals. All the samples contain more vitrinite than inertinite. Some vitrinite and inertinite have well-defined or broken cellular structures (Figure 3b). The samples collected from the northern areas (L1-L2) vary greatly in size of organic matter, while those from the southern areas are dominated by small fragments (Figure 3a-c). Fluorescence was utilized to recognize liptinite, but this is restricted for relatively high mature samples due to fluorescence extinction. Terrestrial liptinite comprises cutinite, resinite, sporinite and part of liptodetrinite (Figure 3d-i). Cutinite includes both thin-wall and thick-wall types. Most spores are dispersed, although some are grouped in sporangiums. The spores have either ornamental or smooth walls (Figure 3 f-i). Besides terrestrial liptinite, fluorescent lamalginite is present in low abundance in the mudstones with T_{max} values<450 ℃ (Figure 3 i-l). Since the samples have entered the oil window, the fluorescence has greatly shifted to the long wavelength (red). When T_{max}>450 °C, the fluorescence intensity of liptinite decreases rapidly and only some spores in dull brown are still identifiable (Figure 3h-i). Fluorescence completely disappears when the T_{max} values exceed 460 °C. No alginite was found in the southern area due to fluorescence extinction.

4.3 SEM observation

Iron sulfides in the mudstones include pyrite and marcasite. Pyrite occurs as framboids, grouped framboidal aggregates, scattered euhedral crystals, or replacements of organic matter (Figure 4a-d). The diameters of the framboids are up to >30 μm (Figure 4a). Pyrite, including some framboids, is usually associated with organic matter or occurs within organic matter (Figure 4b and c). As for the sample L2-S2, framboids are not as abundant as other types of pyrite. Combining DES results and morphology features, abundant needle-like and radial marcasite were identified in L1-S1 and L2-S1 (Figure 4e and f). The spherical shapes of some marcasite clusters indicate that they were formed before compaction (Figure 4f).

4.4 Molecular geochemistry

GC and GC-MS results are present in Table 2 and are also partly shown in Figure 5. Carbon preference index (CPI) reflects the preference of odd- to even-numbered *n*-alkanes in the range of *n*-C_{24-34} (Bray and Evans, 1961). The CPI values of the samples range from 0.99 to 1.23. The terrestrial to aquatic ratios (TAR) values of the mudstones vary from 0.20 to 9.87 (average 3.51), and those of the coals range from 0.30 to 1.54 (average 0.71).

Pristane (Pr) and phytane (Ph) are the most important acyclic isoprenoids. The Pr/Ph values of the mudstones are in the range of 0.76-1.35 and those of the coals range from 0.95 to 2.48. The Pr/*n*-C_{17} and Ph/*n*-C_{18} values of the samples (including the mudstones and the coals) are in the range of 0.17-1.18 and 0.11-0.82, respectively.

Terpane and hopane distributions were obtained from m/z 191 mass fragmentograms (Figure 5). The C_{24} Tet/(C_{24} Tet+C_{23} Tri), C_{24} Tet/(C_{24} Tet+C_{26} Tri) and C_{19} Tet/(C_{19} Tet+C_{23} Tri) ratios are in the range of 0.40-0.99, 0.27-0.94 and 0.13-0.89, respectively. Hopanoids are rich in C_{30} hopane and C_{29} norhopane. The C_{29}/C_{30} hopane ratios of the samples vary from 0.45-1.47. The Ts/(Ts+Tm) values vary from 0.02 to 0.54. The homohopanes comprise C_{31}-C_{35} homohopanes, the concentrations of which decrease with increasing carbon-number. C_{30} moretane/C_{30} hopane ratios range from 0.14 to 0.26. The mudstones generally have larger C_{35}/C_{34} homohopane ratios than the coals. The C_{35}/C_{34} homohopane ratios of the mudstones and the coals are in the range of 0.27-0.64 (average 0.49) and 0.32-0.50 (average 0.4), respectively. As for each pair of homohopanes, the S-isomers predominate over the R-isomers in all the samples. The C_{31} 22S/(S+R) ratios range from 0.54 to 0.60. Gammacerane concentration is relatively low, with the gammacerane indices ranging from 0.03-0.24.

Sterane distributions are shown on m/z 217 mass fragmentograms. The relative proportion of C_{27}, C_{28} and C_{29} regular steranes are in the range of 25-42%, 21-37% and 25-45%, respectively. The C_{29}/C_{27} sterane ratios of the samples range from 0.66 to 1.78. Maturity indices of steranes are C_{29} 20S/(S+R) and C_{29} ββ/(ββ+αα) sterane ratios. The two ratios are in the range of 0.35-0.47 (average 0.42) and 0.35-0.48 (average 0.43), respectively. The hopanes greatly predominate over the steranes, with the sterane/hopane ratios ranging from 0.02-0.58.

5 Discussion

5.1 Organic provenance

The continuous distribution of coal seams, as well as the thin coal laminae in the mudstones, demonstrate a strong input of higher plants. Organic petrographic observation indicates that organic matter of the mudstones is dominated by terrestrial macerals. The samples in the southern areas have much smaller fragments of terrestrial OM than those in the northern areas (Figure 3 a-c), indicating the northern areas are more proximal than the southern areas. In addition, lamalginite is present in low abundance in relatively low mature samples, suggesting an input of aquatic-derived materials. Alginite is not present in the samples in the southern area because these samples have relatively high maturity (T_{max} value>450 °C and R_o>1%), leading to fluorescence extinction. Molecular organic geochemical parameters provide more maturity and provenance information for all the samples.

CPI gives information of provenance, paleo-redox conditions and thermal maturity of organic matter (Bray and Evans, 1961). Petroleum generated from terrigenous organic matter has high CPI values that decreases toward 1.0 with increasing maturation (Peters et al., 2005). Despite the high maturity, our samples have an average CPI value of 1.11 and the value of an individual sample is up to 1.23, suggesting the effects of higher plant inputs. The TAR values of our samples do not well reveal the organic matter sources. The coals which are expected to have high TAR values are found to have extremely low TAR values, even much lower than the mudstones. The low TAR values of the coals are consistent with the short-chain-dominated *n*-alkane distribution (Figure 5). Short-chain-dominated extracts of coals have been reported by previous studies (see also Littke et al., 1990; Zhu et al., 2012; Furmann et al., 2013). Thermal maturation may lead to low TAR values (Zhu et al., 2012). But it is not likely to be the major cause of our samples, since high TAR values occur in a relatively high mature coal, L6-C2, and most of the mudstones. The coals of the Taiyuan and Shanxi Formations in the Linxing Area are rich in vitrinite (> 85%) (Li et al., 2016). It has been found that vitrinite-rich coals contain more short-chain-*n*-alkanes than sporinite-rich coals (Littke et al., 1990). Petersen and Nytoft (2006) also concluded that aliphatic chains >C_{18} are absent from or very restricted in the Carboniferous coals and most of the Permian coals, both of which are vitrinite-rich. Enrichment of short-chain-*n*-alkanes of the samples should result from the retention of more volatile components, which is in agreement with Furmann et al. (2013).

Even though the samples were collected from the underground coal mines, biodegradation may occur in some samples due to the shallow depth (<400 m). *n*-Alkane distribution of some samples comprises unresolved complex mixture (UCM) (Figure 5) and two mudstones have Pr/*n*-C_{17} values >1 (Table 2). However, the large presence of *n*-alkanes indicates that the biodegradation is very slight. Because biodegradation consumes short-chain-*n*-alkanes firstly, paleoenvironmental and paleoclimatic interpretations from biomarkers are effective (Wenger et al., 2002; Izart et al., 2015).

As for non-hopanoid terpenoids, C_{19}-C_{20} tricyclic terpanes are mainly derived from diterpenoids, which are produced by vascular plants (Preston and Edwards, 2000; Hao et al., 2011). C_{24} tetracyclic terpanes are associated with terrigenous organic matter, while relatively high C_{23} tricyclic terpanes are often indicative of aquatic organic matter (Philp and Gilbert, 1986; Peters et al., 1995). C_{24} Tet/(C_{23} Tri+C_{24} Tet) ratios and C_{24} Tet/(C_{26} Tri+ C_{24} Tet) ratios reflect the intensity of terrigenous organic matter input (Hanson et al., 2000; Hao et al., 2011). Figure 6a shows a positive relationship between the two ratios. The two ratios vary substantially, indicating a variable input of terrigenous and aquatic organic matter. The mudstones, except for L2-S1, have moderate values of these ratios,

suggesting a mixed terrigenous and aquatic organic matter input. The relatively high ratios of the coals suggest a predominance of higher plants. Two coals have lower tetracyclic ratios, may indicating more aquatic organic matter components. There is a generally decreasing trend of the two ratios from the Taiyuan Formation to the Shanxi Formation (Figure 6a), indicating increasing aquatic organic matters in this period.

According to previous studies, most bitumen extracts show a clear predominance of C_{30} hopanes, while the predominance of C_{29} hopanes is common for organic matter deposited in anoxic carbonate settings (Philp and Mansuy, 1997). Besides, hopanoids can also be derived from ferns, lichens or mosses, as well as degradation of bacteriohopantetrol (Chaffee et al., 1986; Böcker et al., 2013). C_{29}/C_{30} hopane ratios may increase due to their terrestrial clastic inputs or specialized bacterial community, which attack predominantly sporopollenin substances (Rangel et al., 2002; Zdravkov et al., 2017). Our samples, especially the coals, have relatively high C_{29}/C_{30} hopane ratios. The C_{29}/C_{30} hopane ratios of the mudstones and the coals are up to 0.95 and 1.47, respectively. Abnormally high C_{29}/C_{30} hopane ratios were also reported by Littke and Haven (1989) and Zdravkov et al. (2017). Ferns are common plants in the late Carboniferous to Permian. For example, *Pecopteris* has been reported in formations in the Linxing Area (Qi et al., 2019b). Sterane/hopane ratios reflect inputs of eukaryotic (mainly algae and higher plants) versus prokaryotic (bacteria) organisms (Connan et al., 1986; Cao et al., 2009). In general, high sterane/hopane ratios (≥1) typify marine organic matter with major contributions of algal material (Moldowan et al., 1985). Low sterane/hopane ratios are as a result of a strong bacterial input, and are attributed to the abundant terrestrial materials which contain soil bacteria (French et al., 2014; Song et al., 2017).

As for steroids, it is commonly accepted that C_{29} steranes are mainly sourced from photosynthesizing organisms while C_{27} steranes originate from phytoplankton (Huang and Meinshein, 1979; Moldowan et al., 1985). The moderate C_{29}/C_{27} sterane ratios support a contribution of both aquatic and terrigenous organic matter. The C_{29}/C_{27} sterane ratios show positive relationships with C_{24} Tet/(C_{23} Tri+C_{24} Tet) ratios (Figure 6b), since both of them reflect the intensity of terrigenous organic matter input. However, two of the coals have C_{29}/C_{27} sterane ratios <1, possibly due to aquatic input. Yuana and Zhang (2018) also reported low C_{29}/C_{27} sterane ratios of coals. They concluded that this resulted from the increase in plankton input. The aquatic organic matter inputs of both the mudstones and the coals increase slightly from the Taiyuan to the Shanxi Formations (Figure 6b).

5.2 Validity of sterane biomarker ratios

We saw unusual distributions of m/z 217 mass chromatograms of most of the samples (Figure 7a and b).

Some fragment peaks on m/z 217 mass chromatograms occur at the retention times of hopanes, indicating that they were derived from hopanes (see the peaks marked with inverted triangles in Figure 7a and b). Farrimond et al. (2015) also reported that sterane peaks on m/z 217 mass chromatograms are obscured by hopanes due to high hopane/sterane ratios. The hopane show on m/z 217 mass chromatograms is due to the high hopane to sterane ratios. Signal intensities of the hopanes of the samples are generally one or two orders larger than those of the steranes. In fact, hopanes will produce not only m/z 191 mass fragments, but also relatively low concentrations of other fragment ions, including m/z 217 fragments (see Figure 8.27 in Peters et al. (2005)). Considering the high hopane to sterane ratios, even though a very low proportion of hopanes produce m/z 217 fragments, the concentration of these fragments may be comparable to those of the m/z 217 fragments of steranes.

It is important to check whether the sterane ratios calculated from the m/z 217 mass chromatograms are valid. As for our samples, the hopanes' fragments on m/z 217 mass chromatograms do not affect the identification of steranes' concentration, because the steranes and the hopanes have different retention times. The m/z 217 fragments of steranes and hopanes do not mix with each other. This can be verified through comparing the mass chromatograms between steranes (m/z 217) and hopanes (m/z 191), as well as norhopanes (and m/z 177) (Figure 7). The m/z 217 fragments from hopanes and norhopanes are separate from the sterane peaks on the m/z 217 mass chromatograms. Thus, the sterane biomarker ratios are effective. However, cautions should be taken if the hopanes which have similar retention times with steranes are present in samples.

5.3 Thermal maturity

The T_{max} values (433-470 °C) indicate that the samples are mainly within the oil window (Peters, 1986; Peters et al., 2005), and they generally increase from the north to south. CPI is affected by thermal maturation and paleo-depositional environment. Petroleum generated from terrigenous organic matter has high CPI values which decreases toward 1.0 with thermal maturation (Peters et al., 2005). CPI of the mudstones approaching 1.0 and the low CPI values of the coals indicate that the organic matter is thermally mature. In addition, molecular biomarkers provide more insights into thermal maturity.

Because 17α,21β(H)-hopanes are more thermally stable than 17β,21α(H)-moretanes, C_{30} moretane/C_{30} hopane ratios decrease from 0.8 in immature bitumen to values of <0.15 (typically <0.06) in mature source rocks (Seifert et al., 1979; Mackenzie et al., 1980a; Seifert and Moldowan, 1980; Adegoke et al., 2017). However, the C_{30} moretane/C_{30} hopane ratios of our samples (0.14-0.26) are slightly higher than 0.15, which is inconsistent with their

thermal maturity. It is because that higher terrigenous organic matter inputs from higher plants, peat and coal, and diagenetic effects, often lead to anomalously high C_{30} moretane/C_{30} hopane ratios (Grantham, 1986; Rullkötter and Marzi, 1988; French et al., 2012). In addition, Ts/(Ts+Tm) is regarded as a sensitive maturity indicator but is also controlled by sources, paleoenvironment and lithology (Seifert et al., 1979; Moldowan et al., 1986; Cao et al., 2009). Early diagenesis also plays an important role in setting initial values of Ts/(Ts+Tm) (Moldowan et al., 1986). Because Ts and Tm reach equilibrium at the maturity of R_o ~ 1.4 % (Seifert et al., 1979), Ts/(Ts+Tm) ratios can reflect the variations of maturity of our samples. The Ts/(Ts+Tm) ratios of our samples generally increase with T_{max} values, except for L5-S2 (Figure 8a). Besides, hopane isomerization at C-22 is the most widely applied of hopane maturity parameters. The C_{32} 22S/(22S+22R) ratio reaches equilibrium values of ca. 55-60% over a maturity of 430-436 °C (Farrimond et al., 1998). The hopane maturity ratios of our samples are in the range of 0.54-0.60 and have reached equilibrium, indicating the samples have been thermally mature.

The degree of sterane isomerization is also controlled by thermal degradation. The C_{29} 20S/(20S+20R) and C_{29} ββ/(ββ+αα) sterane ratios are commonly used maturity ratios. The two ratios of our samples are generally larger than 0.4 (Figure 8b), indicating that the samples are thermally mature (Mackenzie et al., 1980a; Difan et al., 1990). However, the C_{29} 20S/(20S+20R) and C_{29} ββ/(ββ+αα) sterane ratios are lower than their expected equilibrium values (0.55 and 0.7, respectively), even though the T_{max} values indicate that part of the samples have reached the late oil window. The m/z 217 mass chromatograms of our samples also clearly show that C_{29} 20R steranes slightly dominate over C_{29} 20S steranes, and C_{29} ααα steranes slightly dominate over C_{29} αββ steranes (Figure 5). Actually, abnormally low sterane maturity ratios have been widely reported for coal measures (see also Dzou et al., 1995; Killops et al., 1998; Norgate et al., 1999; Kotarba and Clayton, 2003; Aderoju and Bend, 2017; Li et al., 2017), because the sterane epimerization ratios are significantly influenced by source input and paleo-depositional environment (Norgate et al., 1999; Aderoju and Bend, 2017). Anomalously low levels of sterane isomerisation is common for coal measures, while anomalously high levels of isomerisation for steranes and homohopanes have been observed occasionally in carbonate hypersaline or high sulfur-content reducing environments (Mackenzie et al., 1980b; Ten Haven et al., 1986; Sun et al., 2016). Besides, reversal of sterane maturity parameters is also a common explanation for abnormally low values of C_{29} 20S/(20S+20R) and C_{29} ββ/(ββ+αα) sterane ratios at relatively high maturity (Lewan et al., 1986; Peters et al., 1990). However, our samples are not likely to be controlled by this regime, since the sterane maturity ratios show no relationship with increasing maturity.

5.4 Hydrocarbon potential

The HI vs T_{max} plot suggests that the mudstones contain both type II and III kerogens (Figure 9a). Compared to the mudstones, the coals and coaly mudstones generally have higher HI values, and are located much above the type III range on the HI vs T_{max} plot (Figure 9a). It has also been recognized that HI vs T_{max} diagrams or HI vs OI diagrams may misrepresent the kerogen types of coals due to the anomalously high hydrocarbon potential of coal samples (Peters, 1986). Jasper et al. (2009) also found that the HI values of the coal are about twice as high as that of the dispersed organic matter, although the maceral composition is similar. One possible explanation to the relatively high HI values of the coals is that coals of higher plant origin (Type III) do not respond to pyrolysis in the same way as dispersed Type III kerogens (Peters, 1986). The reduced HI values of the mudstones are due to the retention of generated hydrocarbons on mineral surfaces during pyrolysis. Additionally, the organic matter is more readily to be oxidized in a mineral-rich environment than in a peat environment (Bostick and Foster, 1975; Scheidt and Littke, 1989; Jasper et al., 2009). Another explanation is that the high HI values result from marine transgression, which is also very reasonable in a transitional phase. Elevated water tabled leads to increased biodegradation, the processing of hydrogen rich components and bacterial lipids to the peat. Excess sulfur from marine water enhances the preservation of hydrogen-rich plant and bacterial lipids through sulfurization (Marshall et al., 2015). Sykes et al. (2014) found that the HI value of marine affected coals is positively correlated with the total S content, which is an indicator of degrees of marine influence (Zieger and Littke, 2019). Anyhow, the coals and coaly mudstones are generally within the band of humic coals (Petersen, 2006) (Figure 9b).

The TOC vs S_2 plot indicates that the samples have poor to excellent hydrocarbon generation potential (Figure 10). The coals have the strongest hydrocarbon potential, followed by the coaly mudstones and then the mudstone samples. The intercalated coal laminae significantly increase the hydrocarbon potential of the mudstones. The predominant terrigenous organic matter input and the presence of liptinite (both terrigenous liptinite and aquatic lamalginite) indicate the source rocks generate mainly gas and may also have oil potential. Many previous studies have discussed the oil generative potential of coals (Horsfield et al., 1988; Littke et al., 1990; Clayton et al., 1991; Hunt, 1991; Powell et al., 1991; Killops et al., 1998; Sykes and Snowdon, 2002; Petersen and Nytoft, 2006). Killops et al. (1998) classified coals into high-H and low-H coals according to H/C ratios. Sykes and Snowdon (2002) evaluated the oil generative potential of the coals by HI values. According to the criteria of Sykes and Snowdon (2002), the coals are in the gas-prone and gas- & oil-prone bands. However, no oil shows can be found in

the formations in the research area. It indicates that the coals did not generate enough oils during maturation to allow migration as a discrete phase. Previous studies also concluded that the Carboniferous and Permian coals have the least oil generative potential, compared with Cenozoic and Jurassic coals (Petersen, 2006; Petersen and Nytoft, 2006).

According to the T_{max} values and the maturity-depended biomarkers, the samples have already been thermally mature, indicating that a certain amount of organic matter has been transformed into hydrocarbon (mainly gas). Stable isotope carbon compositions have verified that the coal measures are the dominant sources of tight gas in the Ordos Basin (Dai et al., 2005; Han et al., 2018).

5.5 Depositional environments

Pristane and phytane are formed from the degradation of chlorophyll phytyl side-chain, which is controlled by the Eh of depositional environments (Didyk et al., 1978). Pr/Ph<1 indicates hypersaline, anoxic or carbonate settings, and Pr/Ph>3 is associated with fluvial, deltaic or humic-dominated sediments deposited under oxic conditions (Mackenzie et al., 1980a; Østensen, 2005). Pr/Ph decreases with thermal maturation. The Pr/Ph ratios of our coals are much lower than common humic coals of similar maturity (Figure 11). The relatively low Pr/Ph values of the coals indicate a strongly marine-influenced sedimentary environment (Ahmed et al., 1999; Yuan and Zhang, 2018). Most of the coal samples have higher Pr/Ph values than the mudstones, suggesting that these coals deposited in a more oxidizing environment (Kotarba and Clayton, 2003). The coalbeds and coal laminae should be formed when proximal depositional settings occasionally transformed into swamp-peat due to sea-level fluctuations. Pr/*n*-C_{17} and Ph/*n*-C_{18} ratios reflect source-rock facies, maturity and biodegradation (Shanmugam, 1985). The two ratios commonly decrease with increasing maturity but increase with biodegradation. This is because isoprenoids break down earlier than *n*-alkanes during maturation and isoprenoids are more bioresistant than *n*-alkanes (Peters et al., 2005). According to the Pr/*n*-C_{17} vs Ph/*n*-C_{18} plot, the mudstones belong to a transitional environment while the coals deposited in both oxidizing and transitional environments (Figure 12a).

The redox conditions are also confirmed by the low gammacerane indices. Gammacerane is generally considered to be derived from tetrahymanol. Water body stratification creates anaerobic conditions where ciliates feed on green and purple sulphur bacteria and produce tetrahymanol because sterols are lacking in their diet (Damsté et al., 1995). Thus, gammacerane is an indicator of stratified water column during sedimentation. High gammacerane indices are commonly associated with hypersaline conditions (Moldowan et al., 1985). Strong

preservation of C_{35} homohopanes is associated with carbonate environments (Seifert et al., 1984). The homohopane indices are positively correlated with the gammacerane indices (Figure 12b), and both the two biomarkers are in low values. Reducing conditions and relatively high salinity commonly have homohopane indices in excess of 5% (Cao et al., 2009; Hu et al., 2019). Thus, the low homohopane indices of our samples (0.01-0.05) support dysoxic to oxic conditions. Both gammacerane indices and homohopane indices increase from the Taiyuan Formation to the Shanxi Formation, indicating increasing reducing conditions. The low gammacerane indices as well as the moderate Pr/Ph ratios of our samples support a dysoxic to oxic condition and a brackish/fresh water body (see also Jiamo et al., 1990).

Pyrite is common in the mudstones, occurring as framboids, grouped framboidal aggregates, scattered euhedral crystals, or replacement of organic matter (Figure 4a-d). Pyrite can be formed in water columns, i.e., syngenetic pyrite, or below sediment-water interfaces, i.e. diagenetic pyrite (Wilkin and Arthur, 2001). Distributions of framboid size are related to the redox conditions of fine-grained sediments (Wilkin et al., 1996). Framboids with a narrow size distribution and maximum size <18 μm are evidence of syngenetic pyrite formation subjacent to the O_2-H_2S boundary (Wilkin and Arthur, 2001). However, the framboids of our mudstone samples vary greatly in size and the diameters are up to ~30 μm (Figure 4a and b), indicating an early diagenetic origin and dysoxic bottom waters. Many framboids and other types of diagenetic pyrite are next to or nested in organic matter (Figure 4b-c), because microbial degradation of organic matter consumes oxygen, forming local reducing conditions. It also indicates limited reducing condition in early depositional period.

Anhedral pyrite replacement (formed by late digenetic pyritization) and dispersive euhedral pyrite (formed via infilling and cementation of previously formed framboids) occur in the mudstones. The lack of syngenetic pyrite and the abundant diagenetic pyrite suggests limited syngenetic pyritization and a less reducing water column (Kortenski and Kostova, 1996; Wilkin et al., 1996; Soliman and El Goresy, 2012; Song et al., 2017). Increases in diagenetic pyrite over framboidal pyrite have been recorded in sediments at basin margins rather than in the more central parts of basins (Wilkin and Arthur, 2001). Beside pyrite, marcasite, the dimorph of pyrite, occurs in L1-S1 and L2-S1. The spherical marcasite in Figure 4f was formed in uncompacted surficial sediments and is a typical early diagenetic marcasite. Early diagenetic marcasite is a reliable indicator of oxygen-bearing bottom waters (Schieber, 2011b). The conclusion obtained from iron sulfides agrees with the biomarkers.

Although the geochemical parameters support a dysoxic and oxic condition, it remains questionable how can such high concentrations of organic matter be preserved in an oxic condition. Organic matter preservation in

sediments are strongly related to oxygen exposure time, namely the time in oxic conditions (Hartnett et al., 1998; Hedges et al., 1999). Thus, the "oxic" records must resulted from short-term exposure to oxic conditions, and the samples which have "oxic" records should have undergone redox oscillations (namely mixed redox conditions). The redox oscillation commonly occurs in coastal and continental margin sediments (Aller, 1994). It results from many mechanisms, including (1) bioturbation and bioirrigation, (2) episodic physical mixing events by upwelling, tidal oscillation and wind-driven waves (Arzayus and Canuel, 2005; Bianchi et al., 2016), (3) seasonal input of rain water (Lewis et al., 2007), (4) diurnal photosynthesis in photic zone (Ivlev, 2015; Peng et al., 2019), (5) variation of intensity of microbial respiration (Bianchi et al., 2016). These events alter the oxygen concentration in bottom waters, moving the redox interface up and down, or directly change the oxygen contents in sediments. Redox oscillations are generally asymmetrical in length and typically spend ~10-100 times longer anoxic than oxic conditions (Aller, 1994), which favors for preservation of organic matter.

Compositions of organic matter are controlled by organic matter sources and altered by oxidative degradation. The oxygen-bearing bottom waters enable selective preservation of terrigenous relative to marine organic matter, because terrigenous fractions are thought to be more resistant to oxidation than marine fractions (Van Santvoort et al., 2002; Burdige, 2005; Huguet et al., 2008). The selective preservation leads to that terrestrial organic carbon has higher burial efficiency than marine organic carbon in transitional zones (Huguet et al., 2008). Thus, the redox conditions of bottom waters partly lead to the enrichment of terrigenous organic matter.

6 Conclusions

(1) Biomarkers and organic petrology suggest a mixed terrigenous and aquatic organic matter input of the mudstones and a dominance of terrigenous organic matter inputs of the coals. The low TAR values of the coals, which result from retention of volatile components, can not reveal the organic precursors of the samples. High hopane concentrations indicate a strong bacterial input.

(2) High hopane to sterane ratios lead to presence of hopane fragment peaks on m/z 217 mass chromatograms. It does not affect the identification of the steranes, because the steranes and the hopanes have different retention times. However, cautions should be taken if the hopanes which have similar retention times with steranes are present in samples.

(3) The T_{max} values and hopane maturity biomarkers indicate that the samples are thermally mature. The C_{30} moretane/C_{30} hopane ratios are higher than expected values for mature samples, which is as a result of the

strong input of terrestrial organic matter. The abnormally low C_{29} 20S/(20S+20R) and C_{29} ββ/(ββ+αα) sterane ratios are due to terrestrial organic matter or coal-related depositional environments.

(4) The coals generally have higher HI values than the mudstones, because minerals in the mudstones will retain the generated hydrocarbons during pyrolysis. Marine influence may also contribute to the high HI values. The TOC vs S_2 plot indicates that the samples have poor to excellent hydrocarbon generation potential. The source rocks produce mainly gases and have poor oil generative potential.

(5) Biomarkers and iron sulfide morphology indicate that the depositional environment is a proximal setting with shallow and brackish/fresh water bodies. The redox indicators support dysoxic to oxic conditions. Since organic matter can not be preserved in oxic conditions, the "oxic" records should resulted from redox oscillations.

Acknowledgements:

This research was financially supported by the National Natural Science Foundation of China (Grant Nos. 41530315, 41872160, 41372213), the National Science and Technology Major Project of China (Grant Nos. 2016ZX05066003, 2016ZX05066006), Strategic Priority Research Program of the Chinese Academy of Sciences (Grant No. XDA05030100), Sichuan Science and Technology Support Program (Grant No. 2016JZ0037), and UK-China Joint Research and Innovation Partnership Fund (Grant No. 201703780094). Valuable comments from Editor Ralf Littke, Reviewer Paul Hackley and the other reviewer are very appreciated. Andrew C. Aplin, Martin Jones and Cees van der Land are also greatly thanked for improving the manuscript and supporting the experiments. Jolanta Kus and Paul Hackley are greatly thanked for identification of alginite.

References:

Adebayo, O.F., Adegoke, A.K., Mustapha, K.A., Adeleye, M.A., Agbaji, A.O., Abidin, N.S.Z., 2018. Paleoenvironmental reconstruction and hydrocarbon potentials of Upper Cretaceous sediments in the Anambra Basin, southeastern Nigeria. International Journal of Coal Geology 192, 56-72.

Adegoke, A.K., Abdullah, W.H., Hakimi, M.H., Sarki Yandoka, B.M., 2015. Geochemical characterisation and organic matter enrichment of Upper Cretaceous Gongila shales from Chad (Bornu) Basin, northeastern Nigeria: Bioproductivity versus anoxia conditions. Journal of Petroleum Science and Engineering 135, 73-87.

Adegoke, A.K., Abdullah, W.H., Sarki Yandoka, B.M., 2017. Provenance and paleoenvironment of organic matter within the Fika sediments in Chad (Bornu) Basin, northeastern Nigeria: An integrated organic geochemical and palynofacies approach. International Journal of Coal Geology 173, 94-109.

Aderoju, T., Bend, S., 2017. A Comparative Assessment of Biomarker-Based Thermal Maturity Parameters. AAPG Memoir 114: Petroleum Systems Analysis—Case Studies, 2017, 219-237.

Ahmed, M., Smith, J.W., George, S.C., 1999. Effects of biodegradation on Australian Permian coals. Organic Geochemistry 30, 1311-1322.
Aller, R.C., 1994. Bioturbation and remineralization of sedimentary organic matter: effects of redox oscillation. Chemical Geology 114, 331-345.
Arzayus, K.M., Canuel, E.A., 2005. Organic matter degradation in sediments of the York River estuary: Effects of biological vs. physical mixing. Geochimica Et Cosmochimica Acta 69, 455-464.
Bianchi, T.S., Schreiner, K.M., Smith, R.W., Burdige, D.J., Woodard, S., Conley, D.J., 2016. Redox Effects on Organic Matter Storage in Coastal Sediments During the Holocene: A Biomarker/Proxy Perspective. Annual Review of Earth and Planetary Sciences 44, 295-319.
Böcker, J., Littke, R., Hartkopf-Fröder, C., Jasper, K., Schwarzbauer, J., 2013. Organic geochemistry of Duckmantian (Pennsylvanian) coals from the Ruhr Basin, western Germany. International Journal of Coal Geology 107, 112-126.
Borrego, A.G., López García, A., Merino-Tomé, O., 2018. Petrographic and geochemical characterization of organic-rich Mississippian black shales in the north of Spain: Vegamián Formation, Cantabrian Zone. International Journal of Coal Geology 190, 126-145.
Bostick, N.H., Foster, J.N., 1975. Comparison of vitrinite reflectance in coal seams and in kerogen of sandstones, shales, and limestones in the same part of a sedimentary section, in: B., A. (Ed.), Petrographie de la matiere organique des sediments, relations avec la paleotemperature et le potentiel petrolier. CNRS, Paris, pp. 13-25.
Bray, E.E., Evans, E.D., 1961. Distribution of n -paraffins as a clue to recognition of source beds. Geochimica Et Cosmochimica Acta 22, 2-15.
Burdige, D.J., 2005. Burial of terrestrial organic matter in marine sediments: A re - assessment. Global Biogeochemical Cycles 19.
Cao, C., Love, G.D., Hays, L.E., Wang, W., Shen, S., Summons, R.E., 2009. Biogeochemical evidence for euxinic oceans and ecological disturbance presaging the end-Permian mass extinction event. Earth and Planetary Science Letters 281, 188-201.
Chaffee, A.L., Hoover, D.S., Johins, R.B., Schweighard, F.K., 1986. Biological markers extractable from coal, in: Johns, R.B. (Ed.), Biological markers in the sedimentary record. Elservier, Amsterdam, pp. 311-345.
Clayton, J.L., Rice, D.D., Michael, G.E., 1991. Oil-generating coals of the San Juan Basin, New Mexico and Colorado, U.S.A. Organic Geochemistry 17, 735-742.
Connan, J., Bouroullec, J., Dessort, D., Albrecht, P., 1986. The microbial input in carbonate-anhydrite facies of a sabkha palaeoenvironment from Guatemala: A molecular approach. Organic Geochemistry 10, 29-50.
Dai, J., Li, J., Luo, X., Zhang, W., Hu, G., Ma, C., Guo, J., Ge, S., 2005. Stable carbon isotope compositions and source rock geochemistry of the giant gas accumulations in the Ordos Basin, China. Organic Geochemistry 36, 1617-1635.
Damsté, J.S.S., Kenig, F., Koopmans, M.P., Köster, J., Schouten, S., Hayes, J., de Leeuw, J.W., 1995. Evidence for gammacerane as an indicator of water column stratification. Geochimica et Cosmochimica Acta 59, 1895-1900.
Darby, B.J., Ritts, B.D., 2002. Mesozoic contractional deformation in the middle of the Asian tectonic collage: the intraplate Western Ordos fold-thrust belt, China. Earth and Planetary Science Letters 205, 13-24.
Didyk, B.M., Simoneit, B.R.T., Brassell, S.C., Eglinton, G., 1978. Organic geochemical indicators of palaeoenvironmental conditions of sedimentation. Nature 272, 216-222.
Difan, H., Jinchao, L., Dajiang, Z., 1990. Maturation sequence of continental crude oils in hydrocarbon basins in China and its significance. Organic Geochemistry 16, 521-529.
Dzou, L.I.P., Noble, R.A., Senftle, J.T., 1995. Maturation effects on absolute biomarker concentration in a suite of coals and associated vitrinite concentrates. Organic Geochemistry 23, 681-697.

Farrimond, P., Naidu, B.S., Burley, S.D., Dolson, J., Whiteley, N., Kothari, V., 2015. Geochemical characterization of oils and their source rocks in the Barmer Basin, Rajasthan, India. Petroleum Geoscience 21, 301-321.
Farrimond, P., Taylor, A., TelnÆs, N., 1998. Biomarker maturity parameters: the role of generation and thermal degradation. Organic Geochemistry 29, 1181-1197.
French, K.L., Sepulveda, J., Trabucho-Alexandre, J., Grocke, D.R., Summons, R.E., 2014. Organic geochemistry of the early Toarcian oceanic anoxic event in Hawsker Bottoms, Yorkshire, England. Earth and Planetary Science Letters 390, 116-127.
French, K.L., Tosca, N.J., Cao, C., Summons, R.E., 2012. Diagenetic and detrital origin of moretane anomalies through the Permian–Triassic boundary. Geochimica et Cosmochimica Acta 84, 104-125.
Furmann, A., Mastalerz, M., Brassell, S.C., Schimmelmann, A., Picardal, F., 2013. Extractability of biomarkers from high- and low-vitrinite coals and its effect on the porosity of coal. International Journal of Coal Geology 107, 141-151.
Ghassal, B.I., Littke, R., El Atfy, H., Sindern, S., Scholtysik, G., El Beialy, S., El Khoriby, E., 2018. Source rock potential and depositional environment of Upper Cretaceous sedimentary rocks, Abu Gharadig Basin, Western Desert, Egypt: An integrated palynological, organic and inorganic geochemical study. International Journal of Coal Geology 186, 14-40.
Grantham, P.J., 1986. Sterane isomerisation and moretane/hopane ratios in crude oils derived from Tertiary source rocks. Organic Geochemistry 9, 293-304.
Hackley, P.C., Fishman, N., Wu, T., Baugher, G., 2016. Organic petrology and geochemistry of mudrocks from the lacustrine Lucaogou Formation, Santanghu Basin, northwest China: Application to lake basin evolution. International Journal of Coal Geology 168, 20-34.
Hakimi, M.H., Ahmed, A.F., 2016. Organic-geochemistry characterization of the Paleogene to Neogene source rocks in the Sayhut subbasin, Gulf of Aden Basin, with emphasis on organic-matter input and petroleum-generation potential. AAPG Bulletin 100, 1749-1774.
Han, W., Ma, W., Tao, S., Huang, S., Hou, Y., Yao, J., 2018. Carbon isotope reversal and its relationship with natural gas origins in the Jingbian gas field, Ordos Basin, China. International Journal of Coal Geology 196, 260-273.
Hanson, A.D., Zhang, S.C., Moldowan, J.M., Liang, D.G., Zhang, B.M., 2000. Molecular organic geochemistry of the Tarim basin, northwest China. Aapg Bulletin 84, 1109-1128.
Hao, F., Zhang, Z., Zou, H., Zhang, Y., Yang, Y., 2011. Origin and mechanism of the formation of the low-oil-saturation Moxizhuang field, Junggar Basin, China: Implication for petroleum exploration in basins having complex histories. AAPG Bulletin 95, 983-1008.
Hartnett, H.E., Keil, R.G., Hedges, J.I., Devol, A.H., 1998. Influence of oxygen exposure time on organic carbon preservation in continental margin sediments. Nature 391, 572-575.
Hasiah, A.W., Abolins, P., 1998. Organic petrological and organic geochemical characterisation of the Tertiary coal-bearing sequence of Batu Arang, Selangor, Malaysia. Journal of Asian Earth Sciences 16, 351-367.
Hedges, J.I., Hu, F.S., Devol, A.H., Hartnett, H.E., Tsamakis, E., Keil, R.G., 1999. Sedimentary organic matter preservation : A test for selective degradation under oxic conditions. american journal of science 299, 529-555.
Holba, A.G., Dzou, L.I., Wood, G.D., Ellis, L., Adam, P., Schaeffer, P., Albrecht, P., Greene, T., Hughes, W.B., 2003. Application of tetracyclic polyprenoids as indicators of input from fresh-brackish water environments. Organic Geochemistry 34, 441-469.
Horsfield, B., Yordy, K.L., Crelling, J.C., 1988. Determining the petroleum-generating potential of coal using organic geochemistry and organic petrology. Organic Geochemistry 13, 121-129.
Hu, G., Meng, Q., Wang, J., XIE, X., LU, L., LUO, H., LIU, W., 2018. The Original Organism Assemblages and Kerogen Carbon Isotopic Compositions of the Early Paleozoic Source Rocks in the Tarim Basin, China. Acta Geologica Sinica - English Edition 92, 2297-2309.
Hu, G., Yang, R., Wang, L., Hu, W., Cao, J., 2019. Hydrocarbon potential and depositional

environment of the Lower Cretaceous black mudstones and shales in the coastal Guangdong Province, China. Marine and Petroleum Geology 99, 92-106.
Huang, W., Meinshein, W., 1979. Sterols as source indicators of organic materials in sediments. Geochim. Cosmochim. Acta 40, 739-745.
Huguet, C., de Lange, G.J., Gustafsson, O., Middelburg, J.J., Damste, J.S.S., Schouten, S., 2008. Selective preservation of soil organic matter in oxidized marine sediments (Madeira Abyssal Plain). Geochimica Et Cosmochimica Acta 72, 6061-6068.
Hunt, J.M., 1991. Generation of gas and oil from coal and other terrestrial organic matter. Organic Geochemistry 17, 673-680.
Ivlev, A.A., 2015. Global redox cycle of biospheric carbon: Interaction of photosynthesis and earth crust processes. Biosystems 137, 1-11.
Izart, A., Suarez-Ruiz, I., Bailey, J., 2015. Paleoclimate reconstruction from petrography and biomarker geochemistry from Permian humic coals in Sydney Coal Basin (Australia). International Journal of Coal Geology 138, 145-157.
Jasper, K., Hartkopf-Fröder, C., Flajs, G., Littke, R., 2010. Evolution of Pennsylvanian (Late Carboniferous) peat swamps of the Ruhr Basin, Germany: Comparison of palynological, coal petrographical and organic geochemical data. International Journal of Coal Geology 83, 346-365.
Jasper, K., Krooss, B.M., Flajs, G., Hartkopf-Fröder, C., Littke, R., 2009. Characteristics of type III kerogen in coal-bearing strata from the Pennsylvanian (Upper Carboniferous) in the Ruhr Basin, Western Germany: Comparison of coals, dispersed organic matter, kerogen concentrates and coal–mineral mixtures. International Journal of Coal Geology 80, 1-19.
Jiamo, F., Guoying, S., Jiayou, X., Eglinton, G., Gowar, A., Rongfen, J., Shanfa, F., Pingan, P., 1990. Application of biological markers in the assessment of paleoenvironments of Chinese non-marine sediments. Organic Geochemistry 16, 769-779.
Ju, Y., Sun, Y., Tan, J., Bu, H., Han, K., Li, X., Fang, L., 2018. The composition, pore structure characterization and deformation mechanism of coal-bearing shales from tectonically altered coalfields in eastern China. Fuel 234, 626-642.
Ju, Y., Wang, G., Bu, H., Li, Q., Yan, Z., 2014. China organic-rich shale geologic features and special shale gas production issues. Journal of Rock Mechanics and Geotechnical Engineering 6, 196-207.
Killops, S.D., Funnell, R.H., Suggate, R.P., Sykes, R., Peters, K.E., Walters, C., Woolhouse, A.D., Weston, R.J., Boudou, J.P., 1998. Predicting generation and expulsion of paraffinic oil from vitrinite-rich coals. Organic Geochemistry 29, 1-21.
Kortenski, J., Kostova, I., 1996. Occurrence and morphology of pyrite in Bulgarian coals. international Journal of Coal Geology 29, 273-290.
Kotarba, M.J., Clayton, J.L., 2003. A stable carbon isotope and biological marker study of Polish bituminous coals and carbonaceous shales. International Journal of Coal Geology 55, 73-94.
Lewan, M.D., Bjorøy, M., Dolcater, D.L., 1986. Effects of thermal maturation on steroid hydrocarbons as determined by hydrous pyrolysis of Phosphoria Retort Shale. Geochimica et Cosmochimica Acta 50, 1977-1987.
Lewis, B.L., Glazer, B.T., Montbriand, P.J., Luther, G.W., Nuzzio, D.B., Deering, T., Ma, S., Theberge, S., 2007. Short-term and interannual variability of redox-sensitive chemical parameters in hypoxic/anoxic bottom waters of the Chesapeake Bay. Marine Chemistry 105, 296-308.
Li, Q., Ju, Y., Chen, P., Sun, Y., Wang, M., Li, X., Chen, J., 2017. Biomarker Study of Depositional Paleoenvironments and Organic Matter Inputs for Permian Coalbearing Strata in the Huaibei Coalfield, East China. Energy & Fuels 31, 3567-3577.
Li, Y., Tang, D.-Z., Xu, H., Qu, Y.-J., Tao, S., Cai, J.-L., 2012. Characterization of coal bearing strata under influence of “seesaw” fulcrum in east margin of Ordos Basin. Journal of China Coal Society 37, 378-382.
Li, Y., Tang, D., Wu, P., Niu, X., Wang, K., Qiao, P., Wang, Z., 2016. Continuous unconventional natural gas accumulations of Carboniferous-Permian coal-bearing strata in the Linxing area,

northeastern Ordos basin, China. Journal of Natural Gas Science and Engineering 36, 314-327.
Li, Y., Yang, J., Pan, Z., Meng, S., Wang, K., Niu, X., 2019. Unconventional Natural Gas Accumulations in Stacked Deposits: A Discussion of Upper Paleozoic Coal-Bearing Strata in the East Margin of the Ordos Basin, China. Acta Geologica Sinica - English Edition 93, 111-129.
Littke, R., Haven, H.L.T., 1989. Palaoecologic trends and petroleum potential of Upper carboniferous coal seams of western Germany as revealed by their petrographic and organic geochemical characteristics. International Journal of Coal Geology 19, 529-574.
Littke, R., Leythaeuser, D., Radke, M., Schaefer, R.G., 1990. Petroleum generation and migration in coal seams of the Carboniferous Ruhr Basin, northwest Germany. Organic Geochemistry 16, 247-258.
Mackenzie, A.S., Patience, R.L., Maxwell, J.R., Vandenbroucke, M., Durand, B., 1980a. Molecular parameters of maturation in the Toarcian shales, Paris Basin, France—I. Changes in the configurations of acyclic isoprenoid alkanes, steranes and triterpanes. Geochimica et Cosmochimica Acta 44, 1709-1721.
Mackenzie, A.S., Quirke, J.M.E., Maxwell, J.R., 1980b. Molecular parameters of maturation in the Toarcian shales, Paris Basin, France—II Evolution of metalloporphyrins. Physics and Chemistry of the Earth 12, 239-248.
Marshall, C., Large, D.J., Meredith, W., Snape, C.E., Uguna, C., Spiro, B.F., Orheim, A., Jochmann, M., Mokogwu, I., Wang, Y., Friis, B., 2015. Geochemistry and petrology of Palaeocene coals from Spitsbergen — Part 1: Oil potential and depositional environment. International Journal of Coal Geology 143, 22-33.
Mathia, E.J., Bowen, L., Thomas, K.M., Aplin, A.C., 2016. Evolution of porosity and pore types in organic-rich, calcareous, Lower Toarcian Posidonia Shale. Marine and Petroleum Geology 75, 117-139.
Meng, S., Li, Y., Wang, L., Wang, K., Pan, Z., 2018. A mathematical model for gas and water production from overlapping fractured coalbed methane and tight gas reservoirs. Journal of Petroleum Science and Engineering 171, 959-973.
Milliken, K.L., Rudnicki, M., Awwiller, D.N., Zhang, T., 2013. Organic matter-hosted pore system, Marcellus Formation (Devonian), Pennsylvania. AAPG Bulletin 97, 177-200.
Moldowan, J.M., Seifert, W.K., Gallegos, E.J., 1985. Relationship between petroleum composition and depositional environment of petroleum source rocks. AAPG bulletin 69, 1255-1268.
Moldowan, J.M., Sundararaman, P., Schoell, M., 1986. Sensitivity of biomarker properties to depositional environment and/or source input in the Lower Toarcian of SW-Germany. Organic Geochemistry 10, 915-926.
Norgate, C.M., Boreham, C.J., Wilkins, A.J., 1999. Changes in hydrocarbon maturity indices with coal rank and type, Buller Coalfield, New Zealand. Organic Geochemistry 30, 985-1010.
Østensen, M., 2005. A geochemical assessment of petroleum from underground oil storage caverns in relation to petroleum from natural reservoirs offshore Norway, Department of Geosciences. University of Oslo, Oslo, Norway.
Peng, C., Bryce, C., Sundman, A., Borch, T., Kappler, A., 2019. Organic Matter Complexation Promotes Fe(II) Oxidation by the Photoautotrophic Fe(II)-Oxidizer Rhodopseudomonas palustris TIE-1. ACS Earth and Space Chemistry 3, 531-536.
Peters, K.E., 1986. Guidelines for Evaluating Petroleum Source Rock Using Programmed Pyrolysis. AAPG Bulletin 70, 318-329.
Peters, K.E., Clark, M.E., Dasgupta, U., Mccaffrey, M.A., Lee, C.Y., 1995. Recognition of an Infracambrian Source-Rock Based on Biomarkers in the Bahewala-1 Oil, India. AAPG Bulletin 79, 1481-1494.
Peters, K.E., Moldowan, J.M., Sundararaman, P., 1990. Effects of hydrous pyrolysis on biomarker thermal maturity parameters: Monterey Phosphatic and Siliceous members. Organic Geochemistry 15, 249-265.

Peters, K.E., Walters, C.C., Moldowan, J.M., 2005. The Biomarker Guide. Cambridge University Press, Cambridge, UK.
Petersen, H.I., 2006. The petroleum generation potential and effective oil window of humic coals related to coal composition and age. International Journal of Coal Geology 67, 221-248.
Petersen, H.I., Hertle, M., Sulsbrück, H., 2017. Upper Jurassic–lowermost Cretaceous marine shale source rocks (Farsund Formation), North Sea: Kerogen composition and quality and the adverse effect of oil-based mud contamination on organic geochemical analyses. International Journal of Coal Geology 173, 26-39.
Petersen, H.I., Nytoft, H.P., 2006. Oil generation capacity of coals as a function of coal age and aliphatic structure. Organic Geochemistry 37, 558-583.
Philp, R.P., Mansuy, L., 1997. Petroleum geochemistry: Concepts, applications, and results. Energy & Fuels 11, 749-760.
Philp, R.t., Gilbert, T., 1986. Biomarker distributions in Australian oils predominantly derived from terrigenous source material. Organic Geochemistry 10, 73-84.
Powell, T.G., Boreham, C.J., Smyth, M., Russell, N., Cook, A.C., 1991. Petroleum source rock assessment in non-marine sequences: pyrolysis and petrographic analysis of Australian coals and carbonaceous shales. Organic Geochemistry 17, 375-394.
Preston, J.C., Edwards, D.S., 2000. The petroleum geochemistry of oils and source rocks from the northern Bonaparte Basin, offshore northern Australia. The APPEA Journal 40, 257-282.
Qi, Y., Ju, Y., Cai, J., Gao, Y., Zhu, H., Hunag, C., Wu, J., Meng, S., Chen, W., 2019a. The effects of solvent extraction on nanoporosity of marine-continental coal and mudstone. Fuel 235, 72-84.
Qi, Y., Ju, Y., Meng, S., Yu, K., Li, W., Jia, T., Wu, J., Chen, W., Luo, L., 2019b. Geological Controls on High Production of Tight Gas in Linxing Block, Eastern Ordos Basin, China. Acta Geologica Sinica - English Edition https://doi.org/10.1111/1755-6724.14334.
Rangel, A., Moldowan, J.M., Nino, C., Parra, P., Giraldo, B.N., 2002. Umir Formation: Organic geochemical and stratigraphic assessment as resource for Middle Magdalena basin oil, Colombia. Aapg Bulletin 86, 2069-2087.
Rickard, D., Luther, G.W., 2007. Chemistry of iron sulfides. Chemical reviews 107, 514-562.
Rullkötter, J., Marzi, R., 1988. Natural and artificial maturation of biological markers in a Toarcian shale from northern Germany. Organic Geochemistry 13, 639-645.
Scheidt, G., Littke, R., 1989. Comparative organic petrology of interlayered sandstones, siltstones, mudstones and coals in the Upper Carboniferous Ruhr basin, Northwest Germany, and their thermal history and methane generation. Geologische Rundschau 78, 375-390.
Schieber, J., 2011a. Iron sulfide formation, Encyclopedia of geobiology. Springer, pp. 486-502.
Schieber, J., 2011b. Marcasite in Black Shales--a Mineral Proxy for Oxygenated Bottom Waters and Intermittent Oxidation of Carbonaceous Muds. Journal of Sedimentary Research 81, 447-458.
Seifert, W.K., Michael Moldowan, J., Demaison, G.J., 1984. Source correlation of biodegraded oils. Organic Geochemistry 6, 633-643.
Seifert, W.K., Moldowan, J.M., 1980. The effect of thermal stress on source-rock quality as measured by hopane stereochemistry. Physics and Chemistry of the Earth 12, 229-237.
Seifert, W.K., Moldowan, J.M., Jones, R., 1979. Application of Biological Marker Chemistry to Petroleum Exploration, 10th World Petroleum Congress. World Petroleum Congress, Bucharest, Romania.
Shanmugam, G., 1985. Significance of coniferous rain forests and related organic matter in generating commercial quantities of oil, Gippsland Basin, Australia. AAPG Bulletin 69, 1241-1254.
Shen, Y., Qin, Y., Wang, G.G.X., Guo, Y., Shen, J., Gu, J., Xiao, Q., Zhang, T., Zhang, C., Tong, G., 2017. Sedimentary control on the formation of a multi-superimposed gas system in the development of key layers in the sequence framework. Marine and Petroleum Geology 88, 268-281.
Soliman, M.F., El Goresy, A., 2012. Framboidal and idiomorphic pyrite in the upper Maastrichtian sedimentary rocks at Gabal Oweina, Nile Valley, Egypt: Formation processes, oxidation products and

genetic implications to the origin of framboidal pyrite. Geochimica Et Cosmochimica Acta 90, 195-220.
Song, J., Littke, R., Weniger, P., 2017. Organic geochemistry of the Lower Toarcian Posidonia Shale in NW Europe. Organic Geochemistry 106, 76-92.
Sun, X., Zhang, T., Sun, Y., Milliken, K.L., Sun, D., 2016. Geochemical evidence of organic matter source input and depositional environments in the lower and upper Eagle Ford Formation, south Texas. Organic Geochemistry 98, 66-81.
Sun, Y.G., Sheng, G.Y., Peng, P., Fu, J.M., 2000. Compound-specific stable carbon isotope analysis as a tool for correlating coal-sourced oils and interbedded shale-sourced oils in coal measures: an example from Turpan basin, north-western China. Organic Geochemistry 31, 1349-1362.
Sykes, R., Snowdon, L.R., 2002. Guidelines for assessing the petroleum potential of coaly source rocks using Rock-Eval pyrolysis. Organic Geochemistry 33, 1441-1455.
Sykes, R., Volk, H., George, S.C., Ahmed, M., Higgs, K.E., Johansen, P.E., Snowdon, L.R., 2014. Marine influence helps preserve the oil potential of coaly source rocks: Eocene Mangahewa Formation, Taranaki Basin, New Zealand. Organic Geochemistry 66, 149-163.
Ten Haven, H., De Leeuw, J., Peakman, T., Maxwell, J., 1986. Anomalies in steroid and hopanoid maturity indices. Geochimica et Cosmochimica Acta 50, 853-855.
Van Santvoort, P.J.M., De Lange, G.J., Thomson, J., Colley, S., Meysman, F.J.R., Slomp, C.P., 2002. Oxidation and origin of organic matter in surficial Eastern Mediterranean hemipelagic sediments. Aquat Geochem 8, 153-175.
Wenger, L.M., Davis, C.L., Isaksen, G.H., 2002. Multiple controls on petroleum biodegradation and impact on oil quality. Spe Reserv Eval Eng 5, 375-383.
Wilkin, R., Barnes, H., Brantley, S., 1996. The size distribution of framboidal pyrite in modern sediments: an indicator of redox conditions. Geochimica et cosmochimica acta 60, 3897-3912.
Wilkin, R.T., Arthur, M.A., 2001. Variations in pyrite texture, sulfur isotope composition, and iron systematics in the Black Sea: Evidence for Late Pleistocene to Holocene excursions of the O2-H2S redox transition. Geochimica et Cosmochimica Acta 65, 1399–1416.
Wilkin, R.T., Arthur, M.A., Dean, W.L., 1997. History of water-column anoxia in the Black Sea indicated by pyrite framboid size distributions. Earth and Planetary Science Letters 148, 517-525.
Wu, P., Hou, D., Gan, J., Li, X., Ding, W., Liang, G., Wu, B., 2018. Paleoenvironment and Controlling Factors of Oligocene Source Rock in the Eastern Deep-Water Area of the Qiongdongnan Basin: Evidences from Organic Geochemistry and Palynology. Energy & Fuels 32, 7423-7437.
Xiao, X.M., Zhao, B.Q., Thu, Z.L., Song, Z.G., Wilkins, R.W.T., 2005. Upper Paleozoic petroleum system, Ordos Basin, China. Marine and Petroleum Geology 22, 945-963.
Yang, Y., Li, W., Ma, L., 2005. Tectonic and stratigraphic controls of hydrocarbon systems in the Ordos basin: A multicycle cratonic basin in central China. AAPG Bulletin 89, 255-269.
Yuan, Q., Zhang, M., 2018. Diversities in biomarker compositions of Carboniferous–Permian humic coals in the Ordos Basin, China. Australian Journal of Earth Sciences 65, 727-739.
Yuana, Q., Zhang, M., 2018. Diversities in biomarker compositions of Carboniferous–Permian humic coals in the Ordos Basin, China. Australian Journal of Earth Sciences 65, 727-739.
Zdravkov, A., Bechtel, A., Sachsenhofer, R.F., Kortenski, J., 2017. Palaeoenvironmental implications of coal formation in Dobrudzha Basin, Bulgaria: Insights from organic petrological and geochemical properties. International Journal of Coal Geology 180, 1-17.
Zhang, K., 1989. Tectonics and Resources of Ordos Fault-Block. Geological Publishing House, Beijing.
Zhu, Y., Li, Y., Zhou, J., Gu, S., 2012. Geochemical characteristics of Tertiary coal-bearing source rocks in Xihu depression, East China Sea basin. Marine and Petroleum Geology 35, 154-165.
Zieger, L., Littke, R., 2019. Bolsovian (Pennsylvanian) tropical peat depositional environments: The example of the Ruhr Basin, Germany. International Journal of Coal Geology 211 https://doi.org/10.1016/j.coal.2019.103209.

Figure 1

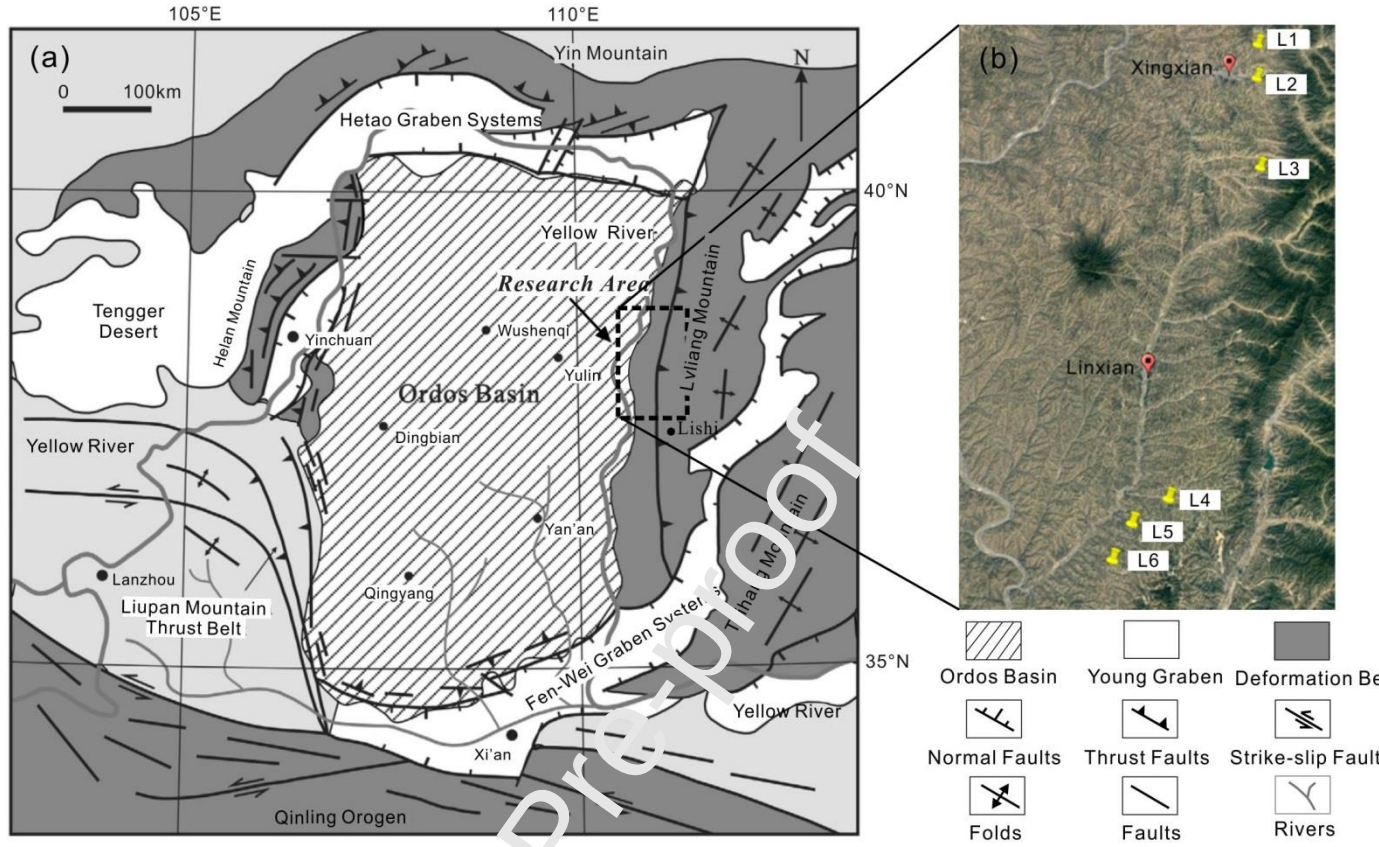

Figure 1 (a) Simplified regional geologic map of the Ordos Basin, after Darby and Ritts (2002). (b) sampling locations in the research area.

Figure 2

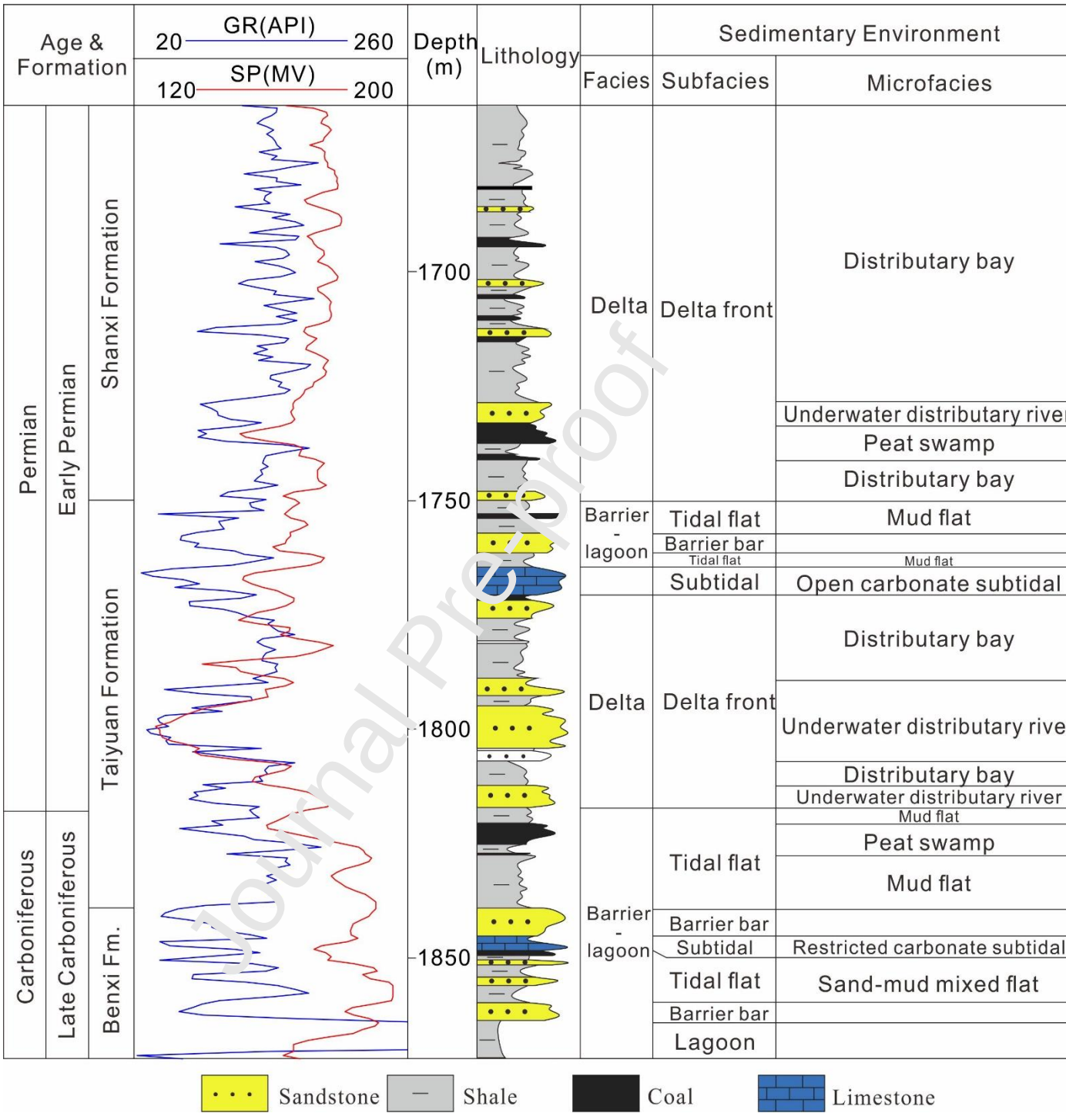

Figure 2 The stratigraphy and sedimentary environment of the Benxi to Shanxi Formations, modified from Shen et al. (2017).

Figure 3

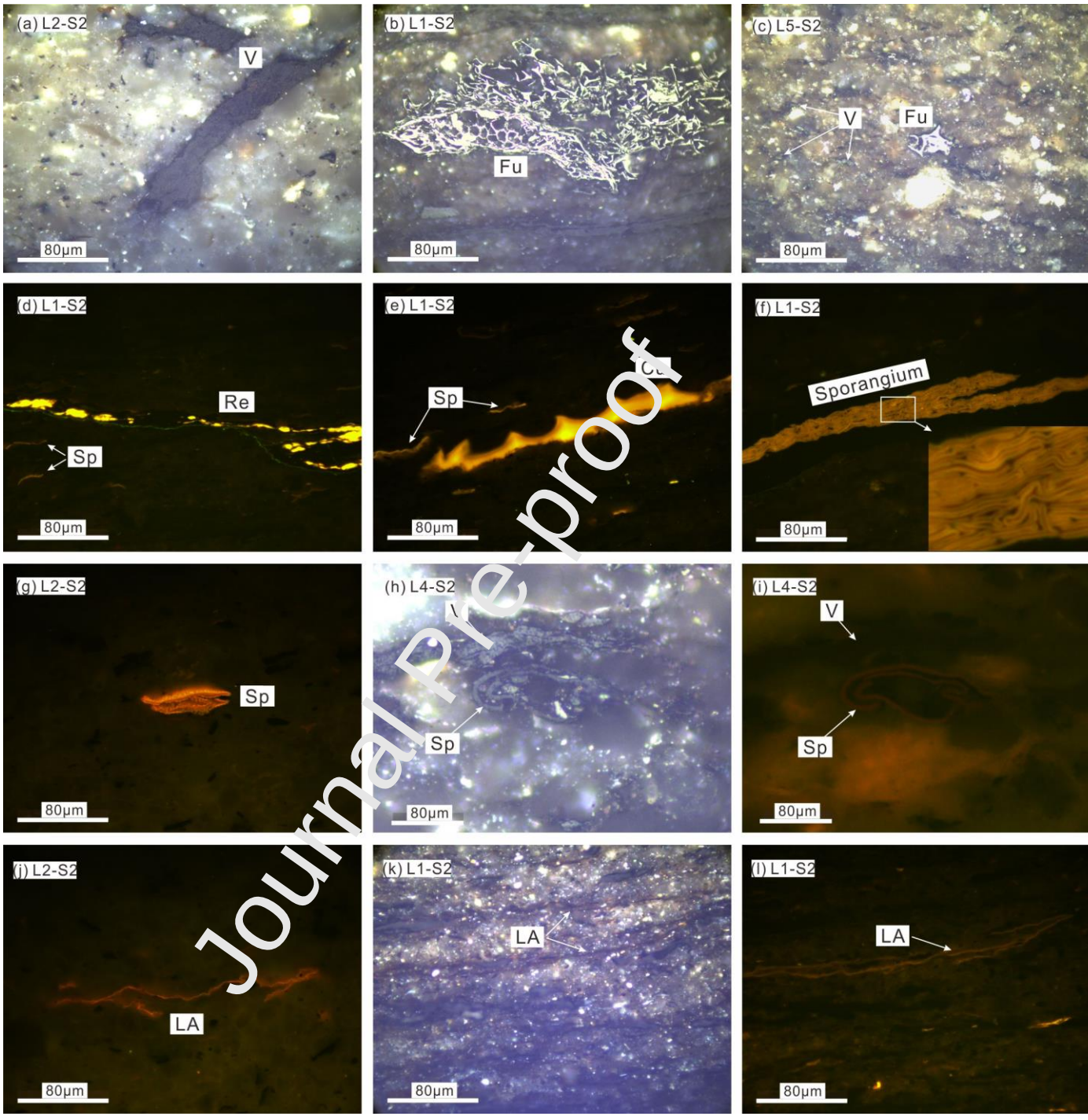

Figure 3 Organic-petrological images. (a), (b), (c), (h) and (k) were taken in fluorescence mode, and others were taken under incident white light. V-vitrinite; Fu-fusinite; I-inertinite; Re-resinite; Sp-sporinite; Cu-cutinite; LA-lamalginite.

Figure 4

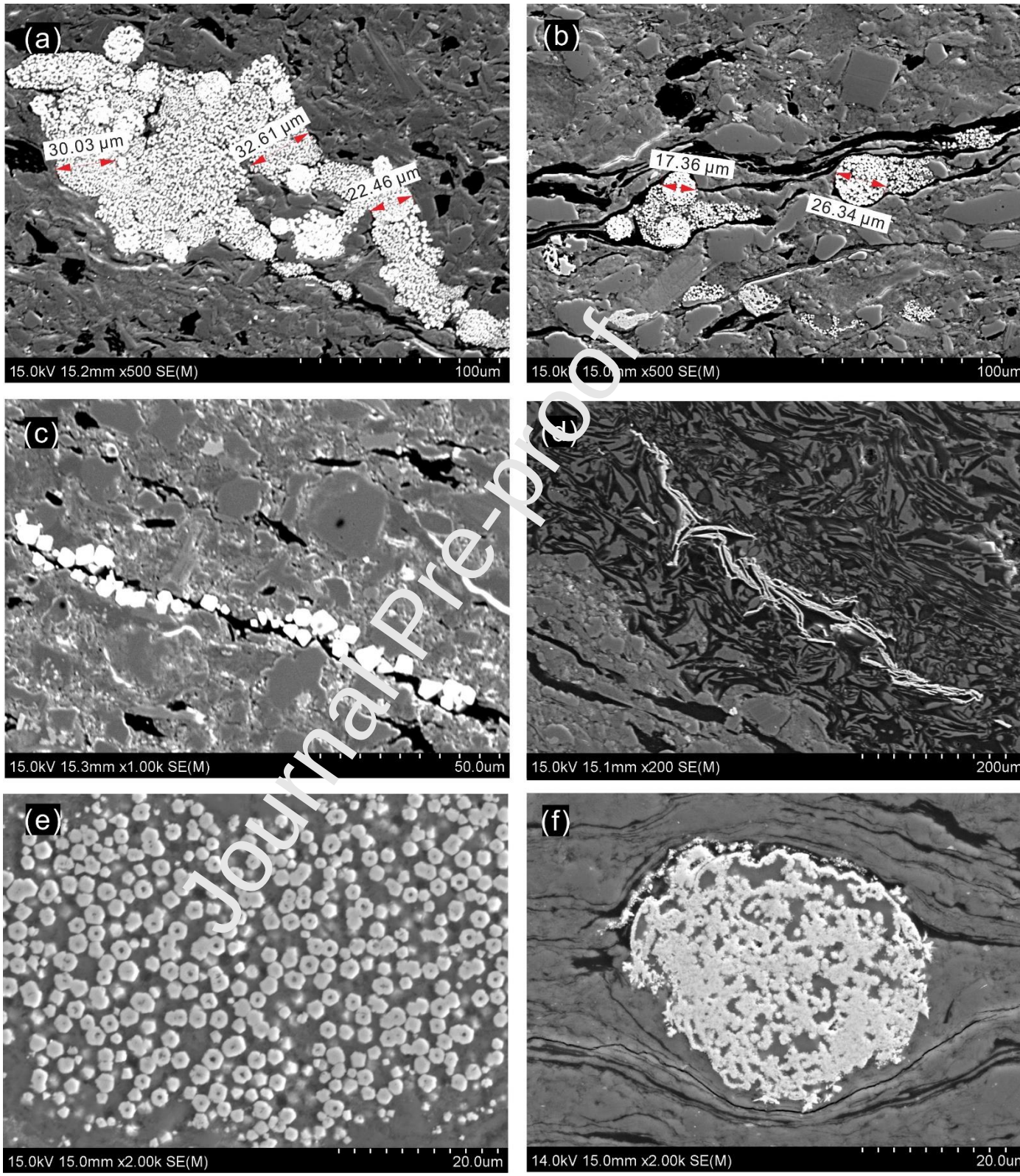

Figure 4 Microscopic morphology of the iron sulfides. (a) L1-S2, grouped framboidal aggregates. (b) L4-S2, framboidal pyrites surrounded by organic matter. (c) L5-S2, euhedral pyrites distributing along organic matter. (d) L1-S2, anhedral pyrite as replacement of organic matter. (e) L1-S1, needle-like marcasite. (f) L2-S1, early digenetic marcasite.

Figure 5

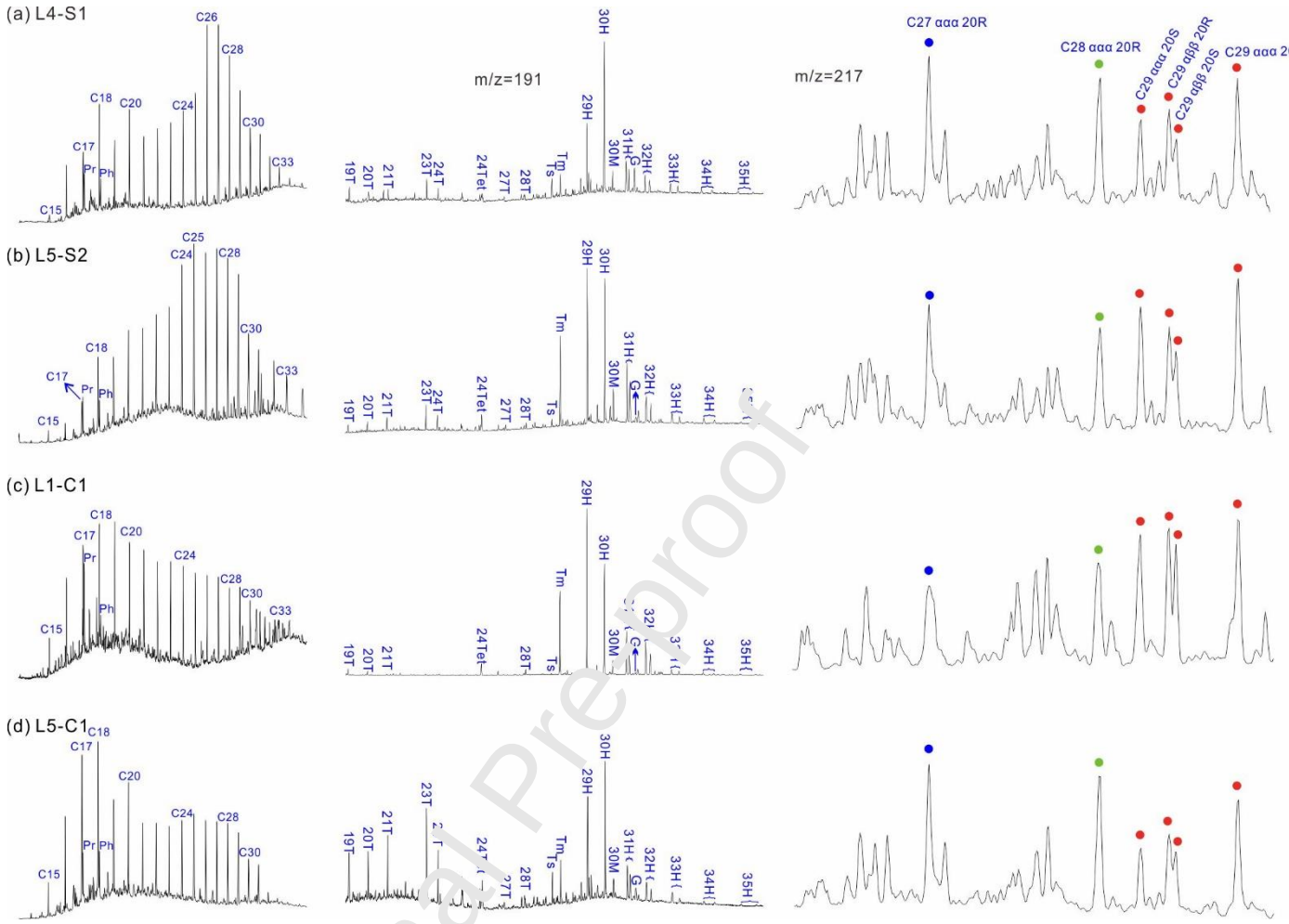

Figure 5 Gas chromatograms and mass chromatograms of terpanes + hopanes (m/z=191) and steranes (m/z=217) of the saturated fraction of extracts derived from two mudstones and two coals.

Figure 6

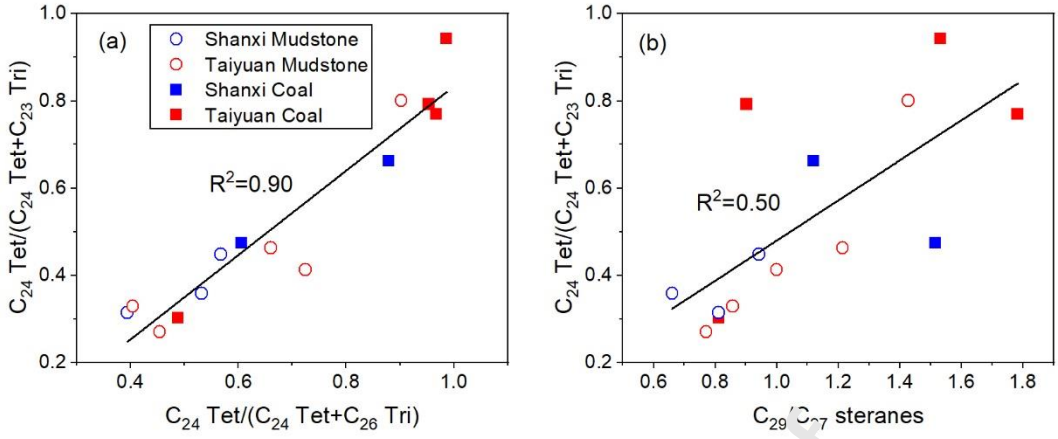

Figure 6 (a) Plot of C_{24} Tet/(C_{24} Tet+C_{23} Tri) ratios vs C_{24} Tet/(C_{24} Tet+C_{26} Tri) ratios. (b) Plot of C_{24} Tet/(C_{24} Tet+C_{23} Tri) ratios vs C_{29}/C_{27} sterane ratios.

Figure 7

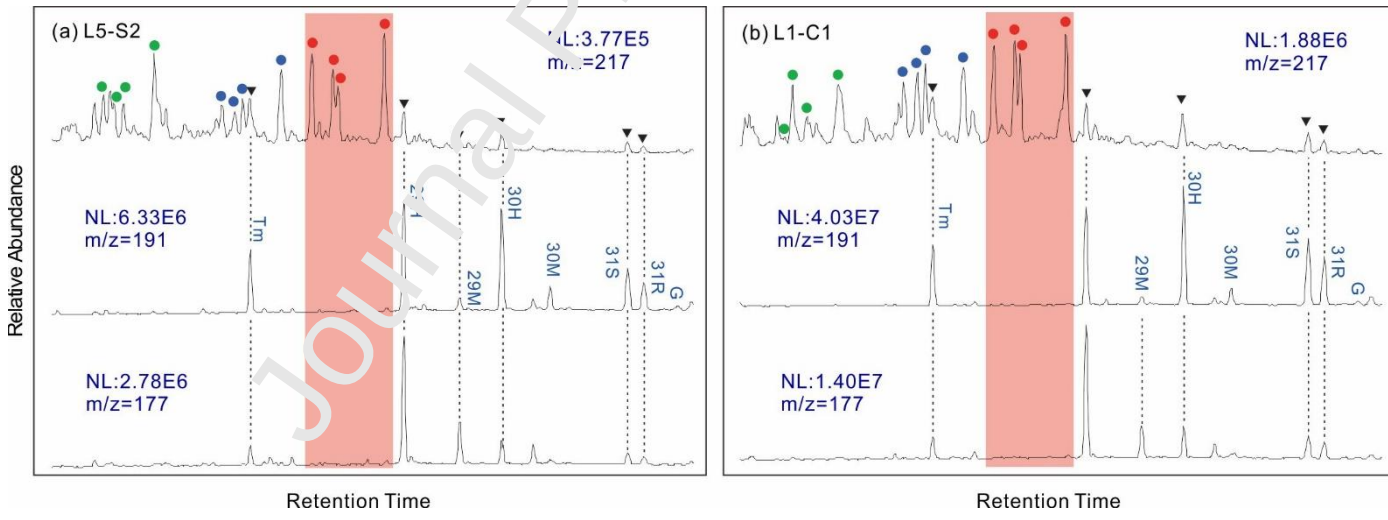

Figure 7 Comparison of m/z 217, 191 and 177 mass chromatograms of L5-S2 and L1-C1. NL represents the nominal level, namely the peak signal intensity. The red, blue and green spots represent the m/z=217 fragments of C_{29}, C_{28} and C_{27} sterane series, respectively. The inverted triangles represent m/z=217 fragments of the hopanes. The red shadow covers the range of the retention times of C_{29} ααα 20S, C_{29} αββ 20S, C_{29} ααα 20R, C_{29} αββ 20R steranes. It indicates that the hopanes and the steranes have different retention times. The hopane-derived fragments do not affect identification of the steranes on m/z 217 mass chromatograms.

Figure 8

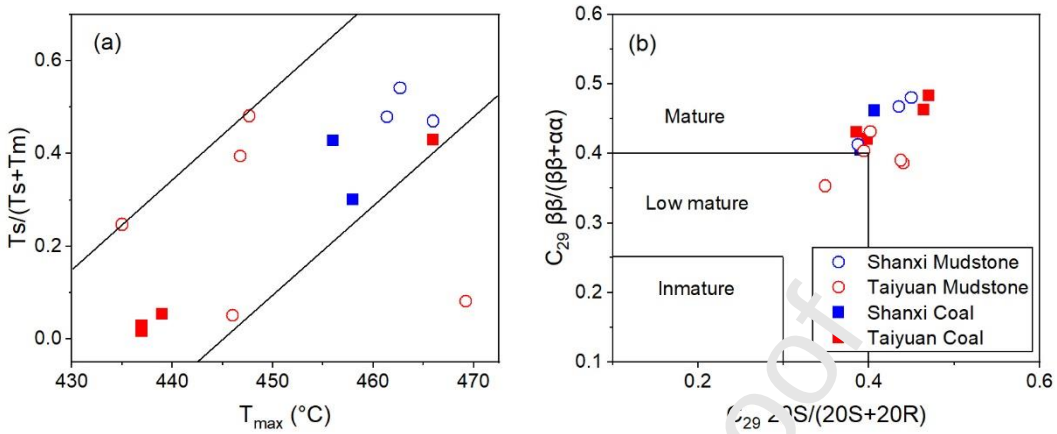

Figure 8 (a) Plot of Ts/(Ts+Tm) ratios vs T_{max} values (b) Plot of sterane maturity ratios.

Figure 9

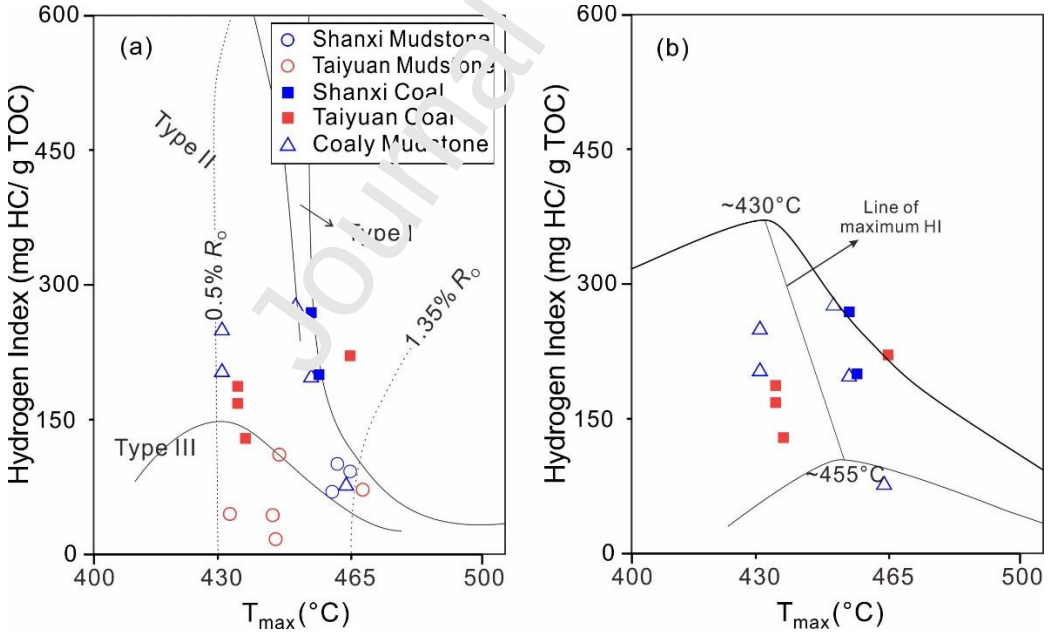

Figure 9 (a) Plot of HI vs T_{max} to determine kerogen types; (b) Plot of HI vs T_{max} with the band of humic coals according to Petersen (2006).

Figure 10

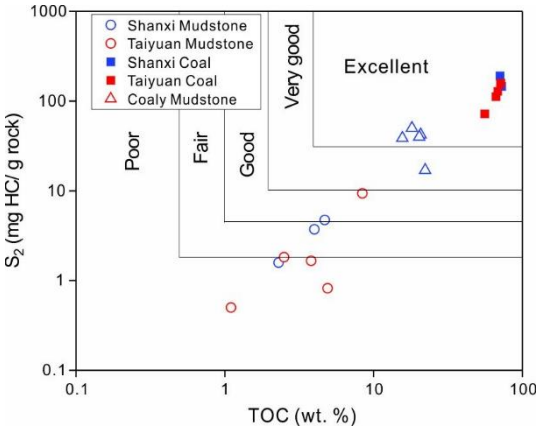

Figure 10 S_2 vs TOC plot to indicate hydrocarbon potential.

Figure 11

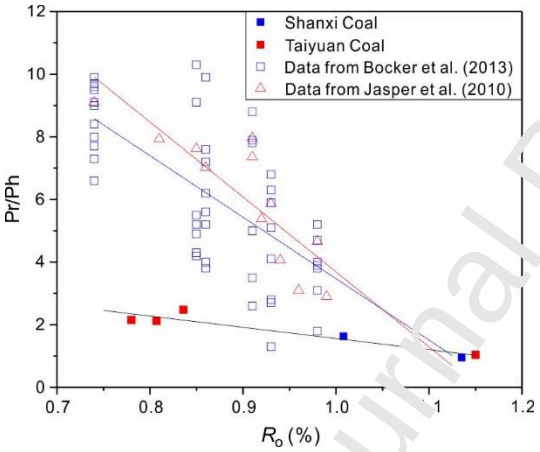

Figure 11 Plot of Pr/Ph vs R_o of the coal samples and data from Jasper et al. (2010); Böcker et al. (2013) (modified from Qi et al. (2019a)). Each group of data are linearly fitted. The fitted lines are in the same color as symbols of corresponding data.

Figure 12

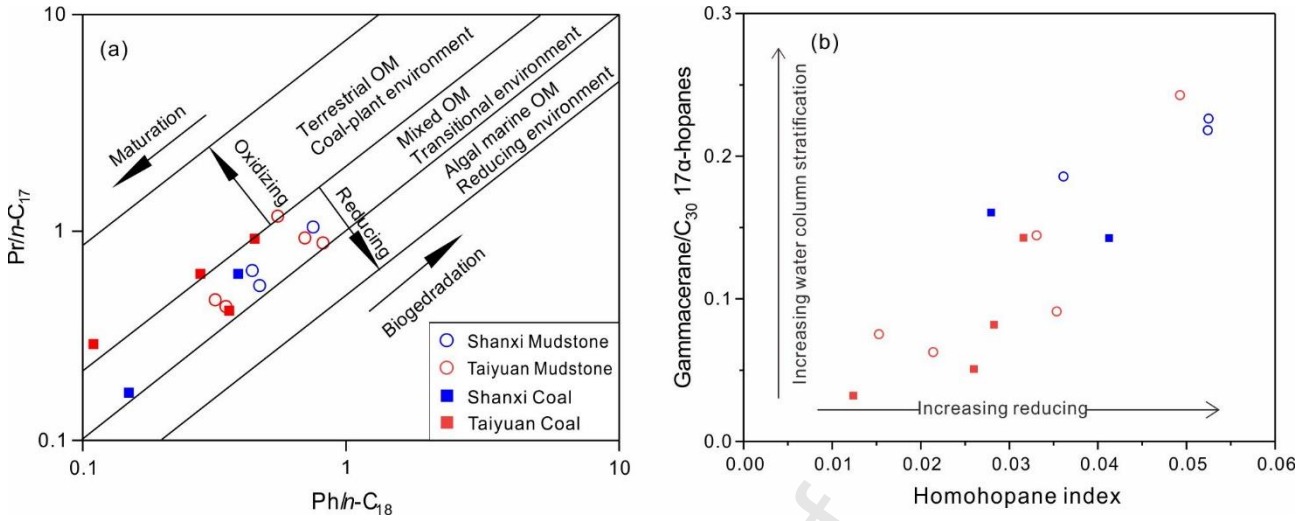

Figure 12 Plots of (a) Pr/*n*-C_{17} vs Ph/*n*-C_{18} and (b) Gammacerane index vs homohopane index.

Tables

Table 1 Sample information, TOC values, Rock-Eval pyrolysis parameters and vitrinite reflectance.

Samples	Lithology	Formation	TOC (wt. %)	T_{max} (℃)	HI (mg/g)	S_1 (mg/g)	S_2 (mg/g)	R_o (%)
L1-S1	Mudstone	Taiyuan	4.9	447	17	0.22	0.82	
L2-S1	Mudstone	Taiyuan	3.8	446	4[illegible]	0.28	1.66	
L2-S2	Mudstone	Taiyuan	1.1	45[illegible]	45	0.02	0.50	
L3-S1	Mudstone	Taiyuan	8.4	448	111	0.48	9.35	
L5-S2	Mudstone	Taiyuan	2.[illegible]	469	72	0.32	1.82	
L4-S1	Mudstone	Shanxi	2.3	461	70	0.36	1.58	
L4-S2	Mudstone	Shanxi	4.0	466	92	0.27	3.72	
L6-S2	Mudstone	Shanxi	4.7	463	101	0.53	4.73	
L1-S2	Coaly mudstone	Shanxi	15.6	433	249	0.22	38.70	
L1-S3	Coaly mudstone	Shanxi	20.7	433	203	0.13	41.94	
L4-S3	Coaly mudstone	Shanxi	18.1	452	276	1.21	49.90	

L4-S4	Coaly mudstone	Shanxi	20.3	456	197	0.93	39.93	
L6-S4	Coaly mudstone	Shanxi	22.2	465	76	0.23	16.93	
L1-C1	Coal	Taiyuan	68.4	437	187	1.65	128.01	0.81
L2-C1	Coal	Taiyuan	66.4	437	168	1.61	111.83	0.78
L3-C1	Coal	Taiyuan	55.8	439	129	1.53	71.78	0.84
L5-C1	Coal	Taiyuan	71.5	466	221	3.31	158.03	1.15
L4-C1	Coal	Shanxi	70.7	456	269	3.61	190.55	1.01
L6-C2	Coal	Shanxi	72.6	458	200	4.26	145.24	1.14

Table 2 Molecular geochemical parameters.

	Samples	L 1-S1	L 2-S1	L 2-S2	L 3-S1	L 5-S2	L 4-S1	L 4-S2	L 6-S2	L 1-C1	L 2-C1	L 3-C1	L 5-C1	L 4-C1	L 6-C2
n-alkanes and isoprenoids	TAR	0.61	3.33	9.87	4.69	0.20	2.20	6.52	0.65	0.18	0.40	0.30	0.77	0.45	1.54
	Pr/Ph	0.76	1.09	0.82	1.23	1.22	1.09	1.10	1.12	2.15	2.48	1.04	1.35	1.63	0.95
	Pr/*n*-C_{17}	0.88	0.47	0.93	1.18	0.65	1.05	0.55	0.92	0.63	0.29	0.42	0.44	0.63	0.17
	Ph/*n*-C_{18}	0.82	0.32	0.70	0.55	0.44	0.75	0.47	0.45	0.28	0.11	0.36	0.35	0.39	0.15
	CPI	1.07	1.23	1.04	0.99	1.05	1.05	1.00	1.11	1.04	1.13	1.15	1.10	1.17	1.19
Terpenoids (Tri)	C_{24} Tet/(C_{24} Tet+C_{23} Tri)	0.33	0.8	0.41	0.46	0.31	0.36	0.45	0.77	0.94	0.79	0.30	0.27	0.66	0.47
	C_{24} Tet/(C_{24} Tet+C_{26} Tri)	0.40	0.9	0.72	0.66	0.39	0.53	0.57	0.97	0.99	0.95	0.49	0.45	0.88	0.61
	C_{19} Tet/(C_{19} Tet+C_{23} Tri)	/	0.67	0.13	0.27	0.48	0.37	0.59	0.61	0.89	0.70	0.39	0.42	0.67	0.34

	Gammacerane index	0	0	0	0	0	0	0	0	0	0	0	0	0	0	0	0
		.14	.08	.09	.06	.23	.19	.22	.05	.03	.08	.14	.24	.16	.14		
	Ts/(Ts+Tm)	0	0	0	0	0	0	0	0	0	0	0	0	0	0	0	0
		.39	.05	.25	.08	.48	.47	.54	.03	.02	.05	.43	.48	.43	.30		
	C_{30} moretane/C_{30}	0	0	0	0	0	0	0	0	0	0	0	0	0	0	0	0
	hopane	.14	.26	.25	.23	.15	.14	.19	.16	.17	.19	.15	.15	.15	.15		
	C_{29}/C_{30} 17α-hopane	0	0	0	0	0	0	0	0	1	1	0	0	0	0	0	0
Hopa		.47	.85	.75	.95	.46	.50	.46	.79	.47	.31	.68	.45	.46	.44		
noids	C_{35}/C_{34} 17α-hopane	0	0	0	0	0	0	0	0	0	0	0	0	0	0	0	0
		.53	.27	.50	.33	.59	.50	.64	.38	.32	.38	.50	.59	.38	.46		
	$C_{32}S/(S+R)$ hopane	0	0	0	0	0	0	0	0	0	0	0	0	0	0	0	0
		.57	.58	.56	.58	.56	.56	.54	.58	.60	.58	.58	.56	.56	.56		
	Homohopane index	0	0	0	0	0	0	0	0	0	0	0	0	0	0	0	0
		.033	015	.035	.021	.053	.036	.052	.026	.012	.028	.032	.049	.028	.041		
	C_{27} ααα 20R(%)	3	3	3	4	3	3	3	3	2	2	4	3	3	2	3	3
		9	1	6	2	3	7	8	6	5	7	1	6	5	5		
Steroi	C_{28} ααα 20R (%)	2	2	2	2	2	3	3	2	3	3	2	3	2	3	2	3
ds		7	4	8	6	7	3	7	9	2	0	1	5	5	6		
	C_{29}ααα 20R (%)	3	4	3	3	4	3	2	3	4	4	3	2	4	3	3	3
		4	5	6	2	0	0	5	4	4	2	7	9	0	9		

C_{29}/C_{27} ααα 20R	0	1	1	0	1	0	0	0	1	1	0	0	1	1					
	.86	.43	.00	.77	.21	.81	.66	.94	.78	.53	.90	.81	.12	.52					
C_{29} ααα	0	0	0	0	0	0	0	0	0	0	0	0	0	0					
20S/(20S+20R)	.39	.44	.35	.44	.39	.44	.45	.47	.46	.40	.39	.40	.41	.39					
C_{29} ββ/(ββ+αα) 20R	0	0	0	0	0	0	0	0	0	0	0	0	0	0					
	.40	.39	.35	.39	.41	.47	.48	.48	.46	.42	.43	.43	.46	.40					
Sterane/Hopane ratio	0	0	0	0	0	0	0	0	0	0	0	0	0	0					
	.20	.03	.25	.11	.24	.37	.28	.16	.02	.02	.58	.23	.22	.15					

Note: TAR, terrestrial to aquatic ratio, (n-C_{27}+n-C_{29}+n-C_{31})/(n-C_{15}+n-C_{17}+n-C_{19}); Tet, Tetracyclic terpane; Tri, Tricyclic terpane; Gammacerane index, Gammacerane/C_{30} 17α-hopane

Highlights

- Terrigenous organic matter dominates the coals and predominates over aquatic organic matter in the mudstones
- High hopane to sterane ratios result in fragment peaks of hopanes on m/z 217 mass chromatograms
- The fragments derived from the hopanes on m/z 217 mass chromatograms do not interfere identification of the steranes
- The redox condition is dysoxic and the oxic records of geochemical parameters result from redox oscillations